High-Resolution Measurements of Integral Cross Sections in Ion–Molecule Reactions from Low-Energy-Guided Crossed-Beam Experiments

Paolo Tosi

Dipartimento di Fisica and Unitá I.N.F.M., Università degli Studi di Trento, I 38050 Povo (TN), Italy

Received March 10, 1992 (Revised Manuscript Received September 21, 1992)

Contents

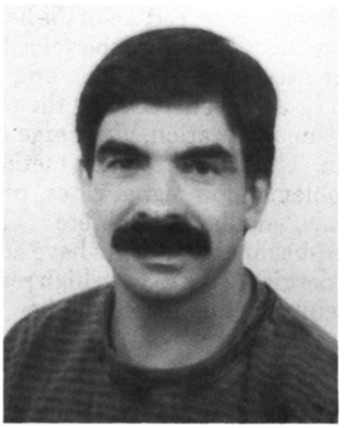

Paolo Tosi was born in Treviso, Italy, on January 26, 1956, and grew up in Padova where he received his degree in Physics in 1980 with a thesis on solid-state spectroscopy carried out at the Institute of Physical Chemistry of the University. His first approach with crossed-beam experiments was in 1984 when he was a visiting scholar at the Department of Chemistry of the University of Utah working in J. H. Futrell's group. In 1985 he got his Ph.D. from the University of Innsbruck (Austria) with a thesis on ion–neutral collisions at low energies. Since 1986 he has been a member of the molecular beam group of the University of Trento, Italy. His current research activity is centered on the dynamics of ion–molecule collisions.

I. Introduction

Several experimental techniques are currently available for measuring the reactivity of ion–molecule systems.[1] The majority of those suitable for exploring low collision energies, the most interesting range from a chemical point of view, yield the rate coefficients k as a function of the relative velocity or temperature. Although k is the key quantity for the chemical kinetics, it does not necessarily lead to detailed information on the elementary mechanisms of chemical reactions. This is due to the fact that k is the average quantity $\langle \sigma v \rangle$ where σ is the cross section, v the relative velocity, and $\langle x \rangle$ indicates the mean value of x.

The average nature of k makes it very difficult to extract the reactive cross section from measurements of the rate coefficient since the maximum available information is limited by the resolving power. In other words several functional forms for the energy dependence of the cross section can fit the experimental rate constants once the average $\langle \sigma v \rangle$ has been performed. Moreover this convolution requires the knowledge of the distribution of reactants' energies.[2] In contrast, the knowledge of the integral reactive cross section as a function of the energy allows the calculation of the equilibrium statistical rate coefficients and any other phenomenological rate coefficient if the corresponding nonequilibrium distribution function is known.[3] On the application side, as in plasma modeling, this is perhaps the most interesting result. From a fundamental point of view, the measurement of the energy dependence of the cross section allows one to probe the potential energy surfaces and to obtain information on the reaction mechanisms by the interplay between experiment and theory. For example, recent progress in theory has suggested the possible detection of resonances in ion–molecule reactions.[4] Although these effects should be more easily detected in differential cross-section measurements, the possibility to scan over the collision energy is in any case a primary experimental requirement.[5] For instance, a few years ago the ability of changing both collision angle and energy allowed the detection of quantum-state specific and angular-specific scattering in the charge-transfer reaction of Ar^+ with N_2.[6] This intriguing observation still challenges theory.[7]

Integral reactive cross sections can be directly measured in beam experiments. This is usually done by allowing a mass and energy selected ion beam to collide with neutral target molecules, contained in a scattering cell at room temperature.[8] Product ions are extracted, mass selected, and finally detected. An advanced version of this technique includes the possibility to select the internal state of the reactant ions.[9] A much higher energy resolution can be reached by using a crossed-beam geometry. This configuration has been extensively used to measure differential cross sections. This topic has been the subject of recent reviews.[10,11,12] Unfortunately low-energy ion-beam experiments suffer

0009-2665/92/0792-1667$10.00/0

of a major drawback: the difficulty of handling an ion beam with an energy below a few electronvolts. For this reason conventional beam experiments have usually explored only the "high" collision energy range, that is energies higher than about 1 eV.

An elegant but technically quite difficult solution to this problem has been given by the development of the merged-beam technique.[13-15] These experiments are based on the idea that very low relative collision energies and high-resolution conditions can be achieved just by merging two high energy (in the kiloelectronvolt region) beams. The reason for making the beams' energy so large lies in the fact that regardless of the electrostatic acceleration, the energy spread ΔE of the beams remains practically constant. Therefore the velocity spread $\Delta v = \Delta E/mv$ decreases by increasing v, and high-energy resolution can be achieved. Usually the neutral beam is produced by neutralization, via charge exchange, of a fast ion beam. Unfortunately, this method gives rise to several problems: low signal rates, production of excited neutrals, angular spread, etc. Therefore, although merged-beam experiments have achieved very low collision energies (2 meV) with high resolution, the intrinsic difficulty of this technique has impeded its widespread use.

An alternative approach, which has become more popular in recent years, is based on the possibility to confine the ion beam in the transverse direction by means of appropriate time-dependent electric fields. In particular, the introduction in the early 1970s of the radio frequency (rf) octopole guides by Teloy and Gerlich[16-18] has revolutionized techniques used to measure integral cross sections at very low collision energies. In fact this device has made possible the production of effective low-energy ion beams, thus giving way to a great number of new experiments.[19] These furnished a great number of data, allowing a great step forward in the field. In particular, the complexity of ion–molecule reactions has been fully appreciated at last, and the general belief that information regarding uninvestigated energy ranges might be deduced from simple models has finally been discarded. A typical example is given by the traditional wisdom that the kinetic energy dependence of exothermic ion–molecule reactions is described by the Langevin model.[20] As sharply emphasized by Armentrout[19] "while a large number of rates seem to conform to the Langevin model, a definitive example of a reaction cross section which shows the predicted dependence on kinetic energy ($\sigma \propto E^{-1/2}$) has been more elusive". As a matter of fact, rather than being simple processes, ion–molecule reactions have usually a complicated dynamics. They are generally controlled by the interaction between the two electronic charge-transfer states of the system, $A^+ + BC$ and $A + BC^+$. Therefore any successful attempt to model these reactions should take into account nonadiabatic effects, going beyond the simple Born–Oppenheimer approximation.

Internal states of the reactants have often proved to play an important role too.[9,21] Besides state-selected experiments, information on the role of the different internal states in determining the reaction dynamics can also be obtained by measuring the energy dependence of the reactive cross section. Whenever kinetic and internal energies are coupled together, these measurements allow the investigation of the role of each internal state over different collision energy ranges.

Unfortunately, most of these experiments have a limited energy resolution due to the distribution of relative velocities created by the thermal motion of the target neutral gas in the scattering cell. Actually this so-called Doppler broadening is important only in the low-energy range (<1 eV), but especially at the lowest energies, its effects are quite severe. As a result the measured cross section differs significantly from the true cross section and any sharp feature is lost.[22] The convolution of the true cross section over the energy distribution of the reactants, as in the case of any experimental determination of the cross section and especially of rate coefficients, might result in a somehow over-simplified and misleading look at the real process. Thus an effort to reach high-resolution conditions at low collision energies might allow the discovery of new effects and stimulate theoretical interpretation.

With this goal in mind a natural development of the rf-guided ion-beam instruments was the replacement of the scattering cell with a supersonic neutral beam. The first successful attempt in this direction was an elegant experiment by Gerlich and co-workers,[23] which was able to show how the reaction of C^+ with molecular hydrogen depends on the initial rotational state of H_2. High-resolution conditions were achieved by crossing at 90° a low-energy-guided ion beam with a pulsed, supersonic hydrogen beam. More recently the same group has developed a new merged–guided-beam apparatus.[18,24] The main difference between the traditional merged-beam method and this new technique is that the latter superimposes a *slow* guided ion beam and a supersonic neutral beam coaxially, instead of two kiloelectronvolt beams as the former does. Interestingly, despite of the low laboratory energies involved, a simple kinematic analysis shows that low collision energies and high-resolution conditions can be reached.[18] As an example, assuming an ion-energy width of 200 meV with an angular spread of 10°, and a well-collimated neutral beam with a speed ratio equal to 40, for the reaction $Ar^+ + H_2$ at the nominal collision energy of 50 meV, the resulting energy spread is 6 meV.

In our group we have developed a new apparatus where a liquid nitrogen cooled, continuous, supersonic molecular beam is crossed at the center of an octopole guide with an ion beam.[17,25-27] This crossed-beam configuration enables an energy resolution to be reached that, in favorable cases, can be 1 order of magnitude higher than experiments using a room temperature scattering cell. For the comparison with the merged-guided ion-beam configuration, there are respective advantages and disadvantages. The merged-beam geometry is superior to the crossed-beam configuration with respect to the lowest accessible collision energy and the possible energy resolution. Other advantages are a larger interaction volume and a more favorable center-of-mass motion. However a major drawback of the merged beam geometry is the poor definition of the interaction region. In fact the two beams overlap not only in the proper scattering region, where the collision energy is well defined, but, in addition, before and after this zone. This raises a variety of problems, mainly due to the fact that the collision energy changes along the whole overlap region.

In this paper recent work of the Trento group is reviewed, with particular emphasis on our effort to reach high-resolution conditions at low collision energies. Hopefully these measurements provide some insight to our understanding of the reaction mechanisms in these systems and in particular of nonadiabatic effects in ion–molecule reactions. Results on the following reactions will be presented and discussed: (1) $Ar^+ + H_2 \rightarrow ArH^+ + H$, (2) $Ar^+ + D_2 \rightarrow ArD^+ + D$, (3) $N_2^+ + H_2 \rightarrow N_2H^+ + H$, (4) $N_2^+ + D_2 \rightarrow N_2D^+ + D$, (5) $Ar^+ + N_2 \rightarrow N_2^+ + Ar$, and (6) $N^+ + D_2 \rightarrow ND^+ + D$.

II. Nonadiabatic Processes: Terminology

Although a wide range of specialized literature is available on this topic,[28] it might be useful to review a few terms to avoid confusion about some otherwise very useful concepts. In this spirit, the aim of this section is not to yield a rigorous treatment of nonadiabatic processes but rather to provide a sort of handbook of definitions of their use.

A. The Adiabatic and Diabatic Representation

Inelastic and reactive molecular collisions are assumed to be governed by potential energy surfaces depending only on nuclear coordinates. The surfaces are often dynamically coupled, especially for processes involving ions. Different reaction channels (e.g. $A^+ + B$ and $A + B^+$) are described at large distance by separate potential energy surfaces, but at shorter range couplings must be introduced. Formally this is done as a matter of convenience, and leads to representations of the adiabatic or diabatic type.

An important characteristic which may simplify the treatment of ion–molecule reactions is that they often depend on long-range forces. Therefore the scattering equations can be formulated as a function of a single coordinate, the distance R between the colliding partners: this is a simplification with respect to reactions where the rearrangement takes place at short range, and the full few body nature of the problem must be taken into account. The role of other coordinates, e.g. those pertaining to molecular vibrations and rotations, are introduced according to appropriate prescriptions: for example, the coupling due to molecular *vibrations* can be often accurately accounted for by Franck–Condon overlap factors. *Rotations* are very difficult to describe exactly, and two limiting cases are often invoked: *sudden* as appropriate at high energy (in this picture molecular relative orientations are considered frozen and then scattering properties are obtained by averaging), and *adiabatically adjusted*, appropriate at low energy (in this regime of slow collisions, it is assumed that the system has sufficient time for molecular relative orientations to adjust to follow the minimum energy path). The latter approach is the one that will be used in the following discussion.

The basic problem in studying a scattering process is then to solve a multichannel Schroedinger equation as a function of R. Alternative approaches to this problem explore respective advantages of different expansions of the total wave function, with the aim to look for partial or full decoupling between the differential equations describing the scattering event. It is therefore important to choose the representation which, at given distances, has the smallest coupling terms. This can be done by exploring the relative importance of different interactions at various distances and selecting the proper representation so that the stronger interactions are represented by nearly diagonal matrices.[29] *The representations such that the matrix of the total potential is not diagonal are called diabatic.*[30,31] The nondiagonal elements are responsible for the coupling between different states. These representations are related by R-independent transformations, often they correspond to different angular momentum coupling schemes (e.g. Hund's cases) and are obviously not unique. By a proper R-dependent transformation it is possible to transfer the coupling from the potential to the kinetic energy operator. *The new representation of the scattering process, obtained by such a transformation, is called adiabatic and is characterized by the fact that the matrix* $\mathbf{V}(R)$ *of the interaction potential is diagonal.* This representation is unique. The physical meaning of the adiabatic description of the scattering process, lies in the coupling between the electronic and nuclear motion, that is electronic transitions are promoted by the nuclear motion. The adiabatic potential curves (in one-dimensional systems) are defined as the elements of $\mathbf{V}(R)$. An important property of these states is given by the *noncrossing rule*: states of the same symmetry do not cross but instead exhibit an avoided crossing (see below).

The adiabatic representation is exact since no approximations have been introduced. On the contrary, by neglecting the coupling terms the *Born–Oppenheimer approximation* is introduced, and in this case the system is described as evolving adiabatically on a single potential energy surface.

B. Adiabatic and Diabatic Behavior

The symmetry of the potential energy surfaces is also important for the dynamical effects of the coupling. Schematically it is possible to distinguish a radial and an angular component of the coupling terms. The radial component couples states of the same symmetry, for example it promotes transitions as Σ–Σ or Π–Π.[32] The angular term, called rotational or Coriolis coupling, is responsible for transitions between states of different symmetry, as for example Σ–Π. In fact the angular term couples the angular momentum of the nuclei with the electronic orbital angular momentum. Note that whereas the radial coupling is very much localized at the avoiding crossing, this is not true for the Coriolis coupling term.

In practice, the proper assignment of the symmetry of surfaces is delicate, because Σ, Π, etc., designations are only valid for collinear approaches and short distances (Hund's cases a and b). We will not give details in the following discussion for the cases under study: it will suffice to say that the Coriolis coupling, typically important at high velocities and high angular momentum, is neglected in our theory of low-energy reactions. Nonadiabatic transitions induced by Coriolis coupling have been discussed in the context of $Kr^+ + H_2$ reaction.[33]

It is important to realize the nature of the adiabatic state before and after the position of the avoided crossing. As a practical example, let us consider the two charge states $A^+ + B$ and $B^+ + A$. If the ionization

potentials of A and B do not differ too much, most probably the two adiabatic potentials, correlating asymptotically with $A^+ + B$ and $B^+ + A$ respectively, exhibit an avoided crossing. This is due to the fact that at this critical distance there exists a mixture of the two charge states. As a consequence $A^+ + B$ is converted to $B^+ + A$ by moving through the avoided crossing on the adiabatic potential. However, the system would maintain its initial charge state by performing a nonadiabatic transition. In this case the system is said to behave diabatically. Therefore *if the system evolves adiabatically through the avoided crossing it changes charge state (e.g. $A^+ + B$ at large distance, $B^+ + A$ at short distance), but it maintains the initial electronic state by evolving diabatically.* Note that these considerations refer to a single passage through the avoided crossing. As an example a charge-transfer reaction involves two passages through the avoided crossing (once in the entrance channel and once in the product channel) but only one nonadiabatic transition.

C. Nonadiabaticity in Ion–Molecule Reactions

As discussed above the charge-transfer reaction is a paradigm of a nonadiabatic collision. However, collisions involving chemical rearrangement may occur, especially at low relative velocities, on a single adiabatic surface. Due to the charge-transfer interaction, most of the ion–molecule adiabatic states exhibit avoided crossings where the interaction between the two charge states becomes strong. As a consequence, a correct description of the reaction dynamics in ion–molecule systems must usually go beyond the Born–Oppenheimer picture, even for such reactions whose products correlate adiabatically with reactants.

As a concrete example let us consider the charged system rare gas–hydrogen, $(Rg–H_2)^+$. Both charge states give $RgH^+ + H$ as products of an H-transfer reaction. Typically the ground state of RgH^+ dissociates to $Rg + H^+$ because of the lower ionization potential of H with respect to that of Rg. Therefore the ground state of the products $RgH^+ + H$ correlates directly with the reactants $H_2^+ + Rg$, whereas it can correlate with the reactants $Rg^+ + H_2$ only via a charge-transfer process.[33,34] The above picture is presumably to be amended for Xe, because of its low ionization potential.[35]

Taking into account the vibrational states of the hydrogen molecule and of the hydrogen molecular ion, several diabatic states have to be considered, each correlating to a vibrational level of the molecules. *These states are called vibronic states.* The dynamical evolution of the system can be understood by localizing the avoided crossings and following the possible adiabatic paths which can lead to products; the nonadiabatic behavior at the crossings dominates the dynamics and must be explicitly taken into account.

III. Energy Broadening

As discussed in the introduction, any real measurement does not yield the "true" cross section $\sigma(E_{CM0})$ at a particular value of the relative collision energy E_{CM0}, but rather its convolution with the kinetic energy distribution of the reactants.

Although obvious, consequences of the previous assertion are often overlooked. As an example let us consider the problem of comparing data obtained in different laboratories. It is evident that a direct comparison is meaningless as the different resolving powers should be taken into account. In particular, it might be completely misleading to compare theoretical calculation results and experimental values. Actually a correct comparison between theory and experiment would require the convolution of the theoretical values on the energy distribution of the particular experiment considered. On the other hand, an exact inversion procedure from experimental quantities to the "true" ones is impossible since, although the energy distribution function would be known, a physical quantity cannot be probed better than permitted by the resolving power of the experiment. This means that features on a scale finer than the energy resolution of the experiment are lost.

A. Beam–Cell Experiments

In most beam experiments, the neutral target gas is contained in a reaction cell. Besides the velocity distribution of the ion beam, a large contribution to the broadening of the relative energy distribution around the nominal value is due to the thermal motion of the neutral gas. This Doppler broadening has been investigated and details can be found in literature.[22,36–38] As an example for the special case of a monoenergetic ion beam (mass m_I) and a neutral molecular gas (mass m_N) at the temperature T, the measured cross section $\sigma_{eff}(E_{CM0})$ is related to the "true" cross section $\sigma(E_{CM0})$ by the convolution integral

$$\sigma_{eff}(E_{CM0}) = \int_0^\infty (E_{CM}/E_{CM0})^{1/2} f(E_{CM},E_{CM0}) \sigma(E_{CM})\, dE_{CM} \quad (1)$$

where $f(E_{CM},E_{CM0})$ is the energy distribution function. The function $f(E_{CM},E_{CM0})$ has an energy spread fwhm (full width at half-maximum) given approximately by

$$\text{fwhm} \approx (11.1\gamma k_B T E_{CM0})^{1/2} \quad (2)$$

where $\gamma = m_I/(m_I + m_N)$ and k_B is the Boltzmann constant.

For $E_{CM0} < k_B T$, the convolution operation is such that the measured cross section is insensitive to the actual form of $\sigma(E_{CM})$. In particular the measured energy dependence of the cross section turns out to be proportional to $E_{CM0}^{-1/2}$ as $E_{CM0} \to 0$. In fact for very low laboratory ion energies, the collision energy is primarily determined by the thermal motion of the neutral molecules, and therefore, the reaction proceeds practically at the thermal rate. As a consequence, the extent to which products are formed depends on the amount of time the reactants interact. Since this period is proportional to the ion velocity, then the rate for products formation is proportional to $E_{CM0}^{-1/2}$. A race toward lower and lower energies in beam–cell experiments is therefore useless, as in any case the dependence $E_{CM0}^{-1/2}$ would be observed, regardless of the true behavior of the cross section. The identity between this phenomenological energy dependence of the cross section and that expected from the Langevin model is of course absolutely casual. Nevertheless one could wonder if the large popularity of this model might be partially due just to this coincidence.

Equation 2 suggests that a way for reducing the Doppler broadening consists in cooling the scattering cell. This possibility has been in fact successfully explored in Armentrout's group[39] using a liquid nitrogen cooled octopole cell. This reduces the width of the energy distribution with respect to a room temperature scattering cell by about a factor of 1.7.

B. Crossed-Beam Experiments

A larger compression of the energy distribution can be achieved by using a supersonic neutral beam as a target. In this case the well-defined kinematics conditions of the reactants allow a very precise definition of the relative velocity. Unfortunately, in a crossed-beam geometry, the relation between improvements in the energy resolution and the signal's intensity is not linear. A rough estimate of the products' signal reduction yields a factor 10^{-4} due to the lower density of molecules in the beam with respect to the scattering cell and a further factor of about 10^{-2}, resulting from the fact that the two beams overlap for a length of about 1 mm; using a cell the interaction region is typically 10 cm long. Therefore a total reduction in the products' signal of about 10^{-6} is expected in a crossed-beam experiment with respect to a beam–cell setup. Moreover adding a molecular beam stage to a tandem mass spectrometer requires more complex experimental machinery.[40]

In our apparatus the two beams are crossed at 90° at the center of the octopole. We define the effective integral cross section σ^*_{eff}, in arbitrary units by

$$\sigma^*_{eff} = S_p/S_0 \tag{3}$$

where S_p and S_0 are the signals of product and primary ions, respectively (with $S_p \ll S_0$). To estimate the true cross section, eq 3 has to be convoluted over the reactants' energy distribution.

This definition of σ^*_{eff} should not be confused with the more used expression given by[25,18]

$$\sigma_{eff} = S_p v_{I0}/S_0 g_0 \tag{4}$$

where g_0 is the nominal relative velocity and v_{I0} the nominal ion laboratory velocity. This latter definition is a first approximation to the true cross section, obtained by neglecting the reactants' energy spread. In other words, σ_{eff} (eq 4) corresponds to the true cross section only in the case of monoenergetic beams.

The cross section is measured as a function of the nominal relative collision energy E_{CM0} by varying the nominal kinetic energy E_{I0} of the ion beam. The relationship between E_{CM0}, E_{I0}, and the nominal kinetic energy of the neutral beam E_{N0} is given by

$$E_{CM0} = (m_N E_{I0} + m_I E_{N0})/(m_N + m_I) \tag{5}$$

where E_{I0} and E_{N0} are both measured in the laboratory reference frame.

The energy E_{N0} of the neutral beam and its distribution can be measured by time of flight methods or calculated considering the enthalpy balance of the supersonic expansion:[41]

$$E_{N0} = {}^5/_2 k_B(T_S - T_{TRANS}) + \int_{T_{ROT}}^{T_S} C_{ROT}(T)\,dT + \int_{T_{VIB}}^{T_S} C_{VIB}(T)\,dT \tag{6}$$

where T_S is the molecular beam source temperature, T_{TRANS}, T_{ROT}, and T_{VIB} are the translational, rotational and vibrational temperatures of the supersonic beam. C_{ROT} and C_{VIB} are the rotational and vibrational contributions to the heat capacity of the neutral gas.

The dependence from the source temperature in eq 6 indicates that to explore very low energies it is important to cool the neutral beam as much as possible.

The energy resolution depends on three distributions which describe the energy spread of the ion and the neutral beams and the angular divergence between the two beams. The resolution can be estimated by a simple error propagation analysis which gives

$$\Delta E_{CM} = \mu[(v_{I0}\Delta v_I)^2 + (v_{N0}\Delta v_N)^2 + (v_{I0}v_{N0}\Delta\phi)^2]^{1/2} \tag{7}$$

where μ is the reduced mass of the system, v indicates the magnitude of the velocity vectors (measured in the laboratory reference frame), ϕ is the angle between the ion and the neutral velocity vectors, and the notation Δx is used to indicate the half width at half maximum (hwhm) of the probability distribution of the quantity x. Note that it is implicitly assumed that the nominal values (indicated by the subscript 0) of the different quantities appearing in eq 7 coincide with the average of the corresponding distribution.

The velocity distribution of the neutral particles for a supersonic beam is

$$f(v_N) \propto {v_N}^3 \exp\left[-\frac{\gamma M^2 (v_N - v_{N0})^2}{2{v_{N0}}^2}\right] \tag{8}$$

where γ is the ratio between the heat capacity at constant pressure and that at constant volume and M is the final Mach number of the supersonic expansion. For sufficiently high Mach numbers:

$$\Delta v_N \simeq \frac{v_{N0}}{M}\sqrt{\frac{2\ln 2}{\gamma}} \simeq \frac{v_{N0}}{M} \tag{9}$$

The width of the energy distribution of the ion beam is measured by the retarding field method (see the section entitled "Experimental") and is in the range $\Delta E_I = 0.1 \sim 0.15$ eV hwhm depending on the specific experimental conditions (E_I is the ion axial kinetic energy). We can write

$$\Delta v_I = \Delta E_I/(m_I v_{I0}) \tag{10}$$

The third term in eq 7 is related to the angular dispersion of the colliding beams. The contribution of the neutral beam is limited by a proper collimation to less than 1 degree. Therefore, only the ionic contribution is important, and it turns out that the main contribution to the energy spread is given by the angular spread of the ion beam.

A significant improvement in the overall energy resolution may be achieved if instead of a crossed-beam arrangement ($\phi = 90°$), a merged-beam configuration ($\phi = 0°$) is adopted.[18] In this case, the angular dispersion affects the energy resolution only in the second order.

From the previous discussion it is clear that the fwhm of the collision energy distribution in a crossed-beam experiment depends on the particular system investigated and on experimental details which, for our apparatus, will be discussed in the next section. Just to give a few numbers, in the case of Ar^+ reacting with H_2 at 50 meV the fwhm in our apparatus is about 16

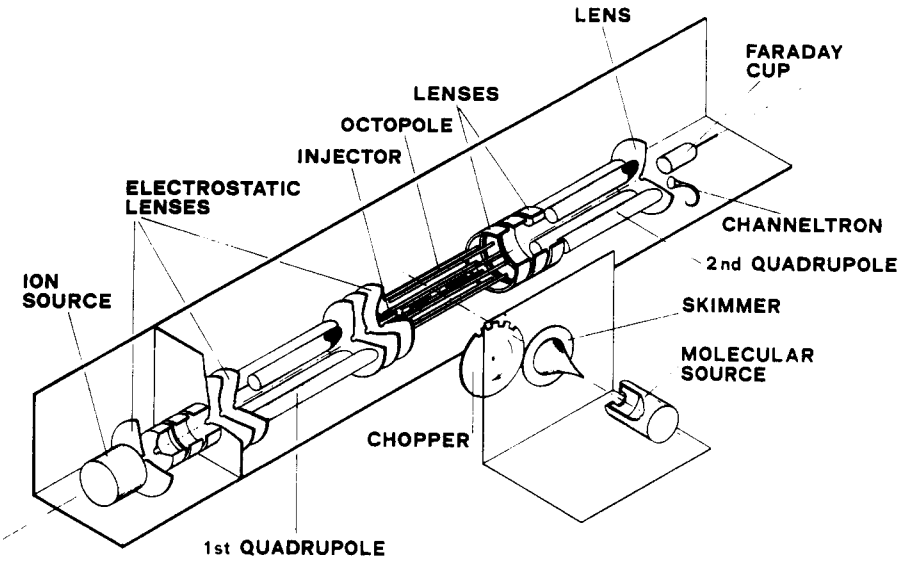

Figure 1. Schematic view of the experimental apparatus. It consists of a guided ion-beam tandem mass spectrometer coupled with a supersonic molecular beam. The two beams cross at 90° in the octopole.

meV. This value compares favorably with a fwhm of 130 meV in the case of a beam–cell setup.

The analog of eq 1 in a crossed-beam experiment is the second integral in dE_{CM} in the following convolution double integral:

$$\sigma^*_{eff}(E_{CM0}) = \int_0^\infty F_1(E_I;E_{CM0}) \times \int_0^\infty \sigma(E_{CM})\beta(E_{CM},E_I)F_2(E_{CM};E_I)\, dE_{CM}\, dE_I \quad (11)$$

where β is given by

$$\beta(E_{CM},E_I) = \sqrt{\frac{(m_I + m_N)E_{CM}}{m_N E_I}} \quad (12)$$

F_2 is the distribution of collision energies E_{CM} when ions have axial energy E_I, whereas F_1 is the distribution function of E_I. F_2 accounts for both the transverse velocity distribution of the ion beam and the velocity distribution of the neutral beam.

The reason to point out the contribution of the *axial* energy of the ion beam via F_1 in the convolution integral, lies in the fact that conventional time-of-flight or retarding-field techniques measure only E_I. The transverse component of the energy can be probed by measuring the ion-beam transmission as a function of the trapping potential[17] or estimated by considering the angular divergency of the ion beam. While F_1 is measured, F_2 has to be calculated numerically by considering the energy spread of the neutral beam and the angular spread of the ion beam.

Besides averaging effects due to the finite energy spread of the two beams, a further "deformation" effect arises from the term β in the convolution integral eq 11. As an extreme but instructive example let us consider the ideal case of two monoenergetic beams with no angular dispersion. F_1 and F_2 are then two delta functions and eq 11 becomes

$$\sigma^*_{eff}(E_{CM0}) = \sigma(E_{CM0})\frac{g_0}{v_{I0}} \quad (13)$$

(Compare with eq 4.) This term accounts for the difference in the residence time of ions in the interaction region at different ion axial energies. As a result the measured cross section is always larger than the true cross section and tends to diverge for very low ion velocities, that is when

$$g_0 \to \sqrt{\frac{2E_{N0}}{m_N}}$$

IV. Experimental

The experimental apparatus is schematically shown in Figure 1. Essentially it consists of a guided-ion-beam tandem mass spectrometer coupled with a supersonic molecular beam. The ion and the molecular beam sources are contained in two separate chambers, each of them pumped by a 2000 L s^{-1} diffusion pump. A third chamber contains the two quadrupole mass spectrometers, the octopole, and the detector. This chamber is pumped by a 300 L s^{-1} turbomolecular pump and a 2000 L s^{-1} cryopump. The typical working pressure ranges from 10^{-6} to 10^{-7} mbar.

The radio frequency octopole is used to guide the primary ion beam at very low velocities and to collect with high efficiency the product ions. Details on radio frequency ion guides are given elsewhere.[17,18] Briefly an octopole guide is a system of eight conductive circular bars arranged with cylindrical symmetry around a central axis. The position of an ion inside the octopole can be described by a system of cylindrical coordinates R, θ, and Z, where Z indicates the position on the symmetry axis and R and θ represent the position in the transverse plane. If a time-dependent electric potential is applied with opposite phase to alternate bars, then the electric potential experienced by the ion is independent from Z and is given by

$$V(R,\theta) = V_0 \cos(4\theta) \cos(2\pi ft)(R/R_0)^4 \quad (14)$$

where R_0 is the (internal) free radius of the octopole, t is the time, f is the frequency, and V_0 is the peak amplitude of the potential applied to each pole. Note that the ion is free in Z while it experiences a force in the radial direction. If the frequency f is sufficiently high the amplitude of the oscillating, fast, motion is small. Nevertheless due to the spatial inhomogeneity

of the time-dependent field, the ion will be attracted toward regions where the field is lower. As a consequence the transverse ion motion can be separated in two terms: a fast one superimposed on a slow one. Under suitable conditions[18] the slow component of the ion motion can be calculated considering an effective, static potential:

$$V_{\text{eff}} = \frac{1}{8\epsilon} q V_0^2 \left(\frac{R}{R_0}\right)^6 \tag{15}$$

where q is the ion charge and ϵ is defined by $\epsilon = {}^1/_8\pi^2 m_I f^2 R_0^2$. This equation shows that a proper time-dependent electric potential acts as an effective potential well. The dependence on R^6 compares favorably with the analog dependence R^2 in the more familiar case of a quadrupole: the trapping potential of an octopole is steeper and it resembles much better the ideal square well. As an example the maximum displacement of an ion starting from the octopole's axis with transverse kinetic energy E_t can be easily calculated from the effective potential (eq 15) using the conservation of energy

$$\frac{R}{R_0} = [8E_t\epsilon/(qV_0)^2]^{1/6} \tag{16}$$

To give a few numbers, in our octopole (8-cm length, 0.45-cm free radius, 10-MHz frequency) an Ar^+ ion with 50-meV transverse energy will be confined inside a maximum distance from the axis of 2.6 mm if a potential $V_0 = 100$ V is applied on the octopole bars. Another ion with double transverse energy (100 meV) will be confined inside 3 mm. Note however that the radio frequency field always perturbs the ion kinetic energy (the transverse component). If the proper working conditions of the octopole are observed,[18] the maximum value of the transverse energy of the ion in the radio frequency field is three times its initial value E_t. This limit can be exceeded for high-field and low-frequency conditions.

The primary ion beam is produced by electron impact. Usually we operate with the lowest useful electron energy and the highest gas pressure ($\approx 10^{-3}$–10^{-2} mbar) to avoid and eventually to quench ion excited states. However different ion sources can be interchanged. Ions extracted from the source are focused by an einzel lens and injected into the first quadrupole where they are mass analyzed. Kinetic energy selection is also possible, making use of the focusing properties of the quadrupole.[18] In practice ions are injected into the quadrupole through a central hole and are then focused on the corresponding exit hole if the number of half cycles inside the octopole is integer. Therefore the transmission through the quadrupole is possible if a precise relation between the quadrupole length and the ion velocity is satisfied: as a consequence ions with a different velocity will not be transmitted. By this technique we can obtain an ion beam of about 10^{-10} A with a fwhm of the energy distribution of about 0.2 eV. A much better energy resolution can be obtained by pulsing the ion beam,[18] unfortunately to the detriment of the duty cycle.

After mass and energy selection, a system of electrostatic lenses transports the ion beam to the octopole. The injection electrode consists of a cylindrical collimator (1-cm length, 0.1-cm internal diameter) which limits the maximum angular divergence of the beam. The ion axial energy distribution is measured by using the octopole to create a retarding field. Aside from simplicity, this method offers several advantages. First of all the trapping potential of the octopole avoids the loss of ions due to focusing effects. This would yield a false retardation curve. Secondly there exists no ambiguity in determining the actual collision energy as the interaction region coincides with that in which the energy analysis is performed. However at very low laboratory energies more reliable results can be obtained by a time-of-flight analysis. A detailed discussion on problems related to the energy calibration can be found in the Gerlich's recent review.[18]

The molecular beam is produced by supersonic expansion, and it enters the reaction chamber through a conical skimmer. It is further collimated in front of the octopole to reduce the angular divergence below about 1°. Due to the small signal-to-noise ratio, a phase-sensitive detection has to be used. The molecular beam is modulated by a mechanical chopper at the frequency of about 600 Hz with a 50% duty cycle and therefore product ions originated in the scattering center are modulated at the same frequency. They are mass selected by a second quadrupole mass spectrometer and finally detected by an electron multiplier. The corresponding signal is measured by means of a homemade digital lock-in amplifier. The chopping frequency is chosen sufficiently high to avoid modulation of the background molecules. Unfortunately this implies that to get an acceptable duty cycle the primary ion beam must be continuous. As a consequence of the practical impossibility to pulse the ion beam, a few systems cannot be investigated with this technique. In particular systems with an unfavorable projectile–target mass ratio may give products which are back-scattered in the laboratory reference frame. The only possibility to collect these ions is then to pulse the primary ion beam and to raise a potential barrier at its entrance immediately after the injection of the ions' burst in the octopole to reflect back to the detector all the ions. Therefore a careful analysis of the scattering kinematics for each system under investigation has to be performed to get reliable results.

V. Survey of Experimental Results

A few examples of our recent work are given in this section, with particular emphasis on those results which show how high resolution measurements may furnish a new insight and stimulate new theoretical models.

A. $Ar^+ + X_2 \rightarrow ArX^+ + X$, X = H, D

The reactions of Ar^+ with molecular hydrogen and deuterium are perhaps the most studied ion molecule reactions.[26,42,43] Early measurements prompted the ion-induced dipole Langevin model.[20] However, recent measurements at low collision energies[22,44–49] have definitely demonstrated that these reactions clearly deviate from the behavior predicted by this model. In particular, the rate coefficient shows a positive energy dependence (see Figure 2).

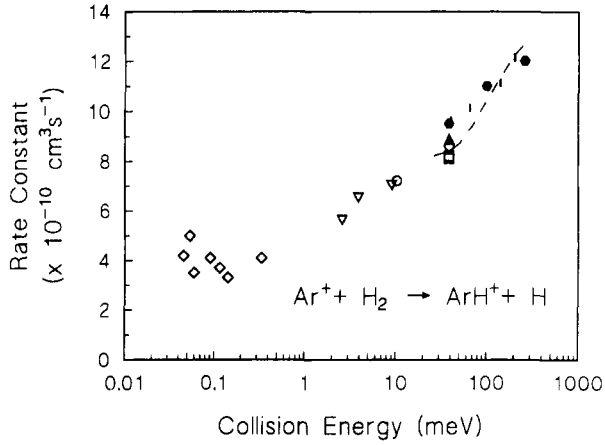

Figure 2. Rate constant as a function of the collision energy for the reaction $Ar^+ + H_2 \rightarrow ArH^+ + H$. Solid hexagons are values obtained by the experimental cross sections of Ervin and Armentrout (ref 22). The dashed line show rate constant values calculated using our measured cross sections (ref 26). The solid triangle is a room temperature value obtained by Smith et al. (ref 44). Open squares are data of Kemper and Bowers (ref 45). Vertical bars are drift-tube measurements of Dotan and Lindinger (ref 46). Open triangles are the low-temperature data of Rebrion et al. (ref 47). Open circles are thermal rate coefficients measured by Bedford and Smith (ref 48). Tilted squares are the very low-temperature measurements of Hawley and Smith (ref 49).

Most of the theoretical analysis has been based on the diatomic-in-molecules (DIM) potential energy surfaces.[34] In particular classical trajectories based on the surface hopping method[50] and quantum calculations[51] have been used to investigate the reaction dynamics of this system. Unfortunately the DIM surfaces do not describe correctly the long-range potential, in particular when a spin–orbit splitting is involved. More recently capture cross sections for this system have been calculated using orientation-averaged adiabatic vibronic potential energy curves.[43]

Taking into account the open-shell nature and the spin–orbit splitting of Ar^+, three potential energy surfaces for the reactants' channel have to be considered, two correlating asymptotically with $Ar^+(^2P_{3/2})$ and one with $Ar^+(^2P_{1/2})$. As already discussed in section II.C, $Ar^+ + X_2$ correlate with the products $ArX^+ + X$ only adiabatically, via the charge-transfer intermediate $X_2^+ + Ar$:

$$Ar^+ + X_2 \rightarrow Ar + X_2^+ \rightarrow ArX^+ + X \qquad (17)$$

In our experiment X_2 is only in the $v = 0$ vibrational state while in the charge-transfer process several vibrational levels of X_2^+ can be populated. As a consequence the vibronic curves related to the different vibrational states of X_2^+ can give effective adiabatic paths to the reaction and it is expected that by varying the collision energy the progressive openings of these paths should be observed, see Figure 7. Therefore by measuring the cross section versus the collision energy, the onsets of successive reaction channels should be detected. This idea develops a result obtained in the 1970s by Baer and Beswick.[52] In fact, these authors calculated a threshold at about 0.06 eV, corresponding to a barrier arising from the crossing between the curve $v = 0$ of $Ar^+ + H_2$ and $v = 2$ of $H_2^+ + Ar$.

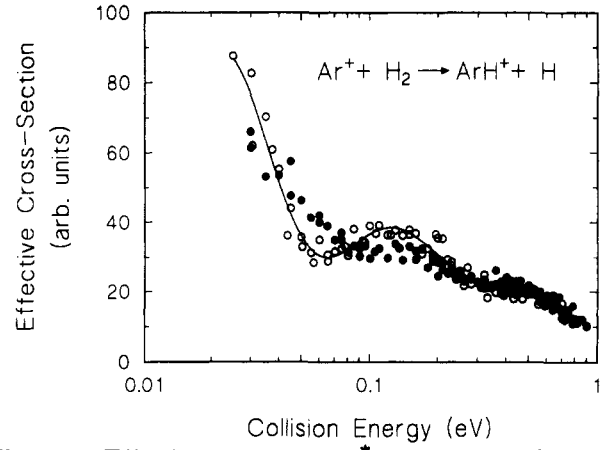

Figure 3. Effective cross section σ^*_{eff} (see eq 3) as a function of the collision energy for the reaction $Ar^+ + H_2 \rightarrow ArH^+ + H$. Open circles are obtained using an Ar^+ beam with an energy spread of 0.2 eV fwhm. Solid circles are obtained using an Ar^+ beam with an energy spread of 0.7 eV fwhm.

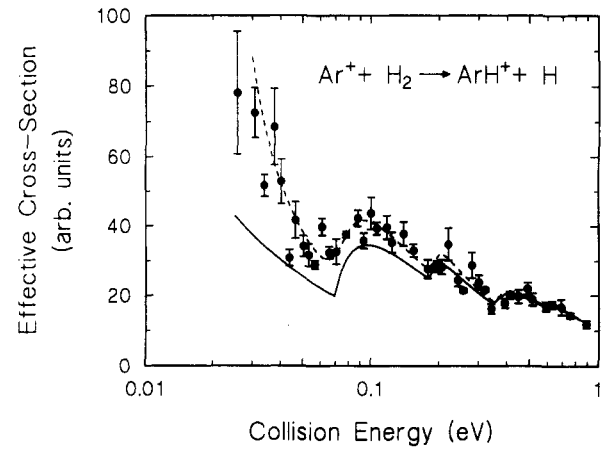

Figure 4. Circles are the effective cross sections (see eq 3) as a function of the collision energy for the reaction $Ar^+ + H_2 \rightarrow ArH^+ + H$. The solid line is a parametrized function (see eq 18). The dashed line is its convolution with the energy distribution of the reactants in the present experiment.

The experimental detection of such thresholds may be possible only if the resolving power of the experiment is sufficiently high to discriminate structure of the order of the vibrational spacing of X_2^+. In Figure 3 we report effective cross sections as a function of the collision energy for the $Ar^+ + H_2 \rightarrow ArH^+ + H$ reaction. These values result from two measurements in which ion beams with different energy distribution have been used (open circles correspond to an energy spread of 0.2-eV fwhm while solid circles correspond to 0.7-eV fwhm in the laboratory reference frame). By using ion beams with different energy spread, we can investigate how possible features are affected by the energy resolution. The high-resolution set shows a clear structure which, following the previous arguments, is attributed to the successive onset of reaction channels with an energy barrier. However in the low-resolution data the low-energy feature is completely lost.

Experimental results (given by eq 3) for the energy dependence of the cross section, averaged over several data sets, are reported in Figures 4 and 5 for the hydrogen and deuterium reaction, respectively. Following the discussion in section III, in order to compare these values with those obtained by other laboratories, in the case of hydrogen we have introduced a trial

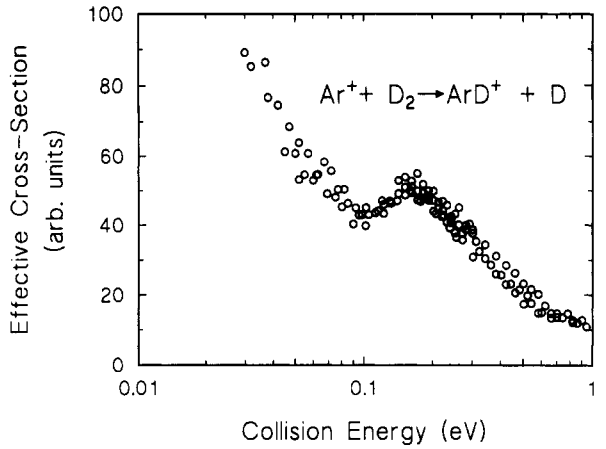

Figure 5. Effective cross section (see eq 3) as a function of the collision energy for the reaction $Ar^+ + D_2 \rightarrow ArD^+ + D$.

function, shown in Figure 4 as a full line, for $\sigma(E_{CM0})$:

$$\sigma(E_{CM0}) = \sum_{j=1}^{k} \alpha_j (E_{CM0} - E_j)^{N_j} / {E_{CM0}}^{M_j} \qquad (18)$$

with $E_{CM0} \geq E_j$.

This form has been extensively used in literature.[53] Each term in the sum describes the opening of the endothermic channel with energy threshold E_j. Free parameters are optimized by fitting the experimental data after convolution with eq 11.

Equation 18 is an approximation to the true cross section and can be used to explore the effect of the reactants' energy distribution on the experimental output. As an example in Figure 6 we show results obtained by convoluting the function $\sigma(E_{CM0})$ with the energy distribution of a beam–cell experiment at room temperature. This figure indicates that, as already discussed in section III, although the cross section has a monotonic energy dependence, the low-resolution measured cross section has practically a monotonic behavior. The same form can be used to calculate rate constants k as a function of temperature, T:

$$k(T) = \frac{1}{k_B T}\sqrt{\frac{8}{\pi\mu k_B T}}\int_0^\infty \sigma(E_{CM})E_{CM} \times \exp(-E_{CM}/k_B T)\, dE_{CM} \qquad (19)$$

Results of this calculation are shown in Figure 2 and indicate that the general energy dependence measured in our apparatus is in good agreement with that measured in other laboratories.

In a continuous collaboration between Aquilanti's group at the University of Perugia and ours,[26,54,55] a full treatment of the dynamics of these reactions has been developed.

The starting point was the new estimate of the potential energy surfaces for the $Ar^+ + X_2$ systems in order to explicitly account for the fine structure and vibrational effects. Fine structure effects have been observed experimentally:[42,49,56,57] in particular the higher reactivity of $Ar^+(^2P_{1/2})$ as compared to $Ar^+(^2P_{3/2})$ has been demonstrated. Moreover an interesting isotopic effect has been observed, but not yet understood, for the reaction of the $^1/_2$ state.[49,56] In fact the reactivity of this state with respect to that of the $^3/_2$ state is higher for H_2 than for D_2.

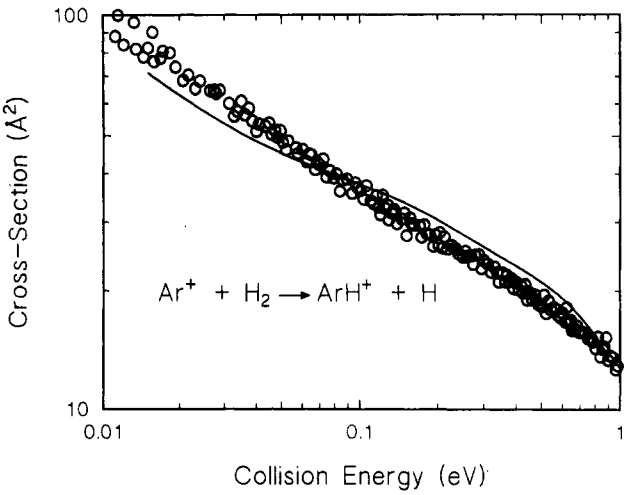

Figure 6. Circles are experimental results of ref 22. The line represents results of the integration of eq 18 (solid line in Figure 4) over the energy distribution of a beam–cell experiment (see eq 1).

For the entrance channel $Ar^+ + X_2$, the effective adiabatic potentials $V_{J\Omega}(R)$ (R is the distance between the ion and the center of mass of the molecule and Ω is the absolute projection of the total angular momentum J along R) are represented by the following formulas:[29,58]

$$V_{3/2,3/2} = V_0 - {}^1/_5 V_2 \qquad (20)$$

$$V_{3/2,1/2} = V_0 + {}^1/_{10} V_2 + {}^1/_2\Delta - {}^1/_2\left(\frac{9}{25}V_2^2 + \Delta^2 - {}^2/_5 V_2\Delta\right)^{1/2} \qquad (21)$$

$$V_{1/2,1/2} = V_0 + {}^1/_{10} V_2 + {}^1/_2\Delta + {}^1/_2\left(\frac{9}{25}V_2^2 + \Delta^2 - {}^2/_5 V_2\Delta\right)^{1/2} \qquad (22)$$

where Δ is the spin–orbit splitting and $V_0(R)$ and $V_2(R)$ represent, respectively, the spherical and anisotropic components of the electrostatic interaction.

The main contribution to $V_0(R)$, which is of the charge-induced dipole type for the long-range attraction, has been estimated by making use of recently developed empirical correlations.[59,60] These correlations have proven useful in predicting reliable potential parameters when van der Waals forces are operative and specific chemical contributions are absent.

$V_2(R)$ is determined by the electronic anisotropy term, arising from the open-shell nature and spin–orbit splitting in $Ar^+(^2P_{3/2,1/2})$.[58] In fact, at short distances the electrostatic interaction is strong enough to decouple the atomic spin–orbit coupling. Now $J = 1/2,3/2$ is no longer a good quantum number and therefore it has to be substituted by the projection of the electronic angular momentum L on the intermolecular axis. In the case of Ar^+, $L = 1$ and therefore we obtain three surfaces, $1\ ^2A'$, $1\ ^2A''$, $2\ ^2A'$ which, in the two-body asymptotic limit, can be given the collinear designations $^2\Sigma_{1/2}$, $^2\Pi_{3/2}$, and $^2\Pi_{1/2}$, respectively.[58] The state Σ corresponds to the case when the atomic orbital of Ar^+ which contains the odd electron, p_z, points toward X_2 while the two Π states correspond to the in-plane and out-plane perpendicular orientations of p_z with respect to the

intermolecular axis. Therefore the anisotropy term accounts for the effects due to orientation of the p_z orbital of Ar^+ with respect to the Ar^+–X_2 axis. The magnitude of the anisotropy term is expected to depend inversely on the difference between the ionization potentials of the two colliding particles. In fact for small differences the odd electron can be delocalized, and this effect depends on the orientation of the half filled orbital p_z. The conservation of the quantum number Ω, which at large distances tend to $|m_J|$, allows one to correlate the asymptotic $Ar^+(^2P_{3/2}) + X_2$ state with the short distance $^2\Sigma_{1/2}$ and $^2\Pi_{3/2}$ states resulting in the $V_{3/2,1/2}$ and $V_{3/2,3/2}$ surfaces and $Ar^+(^2P_{1/2}) + X_2$ with the $^2\Pi_{1/2}$ state yielding the $V_{1/2,1/2}$ surface. Therefore an important effect, due to the spin–orbit interaction, is the partial mixing of Σ and Π characters in the adiabatic surfaces at large and intermediate distances. In particular it is possible to show that while $V_{3/2,3/2}$ has a pure Π character, the $V_{3/2,1/2}$ and $V_{1/2,1/2}$ potentials acquire pure Σ and pure Π character, respectively, only at short distances.[55]

For the intermediate charge-transfer complex in the collinear configuration (assumed to provide the lowest reaction paths with no activation energy) we have considered both charge-induced dipole and dispersion attractions, as well as a repulsive term due to the configuration interaction.[55,61] However several surfaces for this intermediate complex have to be considered, corresponding to the possible vibrational quanta v of X_2^+.

Collinear cuts to the proposed potential energy surfaces are shown in Figure 7. By symmetry considerations, that is taking into account that the charge-transfer intermediate has essentially a Σ character in the collinear configuration, it is possible to identify the crossings which are avoided and therefore may lead to efficient adiabatic behavior.[55] They are circled in Figure 7. Since only Σ–Σ-type crossings are assumed to be avoided, the $V_{3/2,3/2}$ surface is not reactive and therefore in this model one-third of Ar^+ ions never react with X_2. However a minor contribution to the reactivity, here neglected, may arise from Coriolis coupling at large impact parameters.

The identification of the relevant avoided crossings offers a straightforward explanation for the fact that the ratio between the $J = 1/2$ and the $J = 3/2$ cross sections is larger in the case of H_2 than in the case of D_2.[49,56] The 1/2 state reacts with H_2 through an external crossing at about 5 Å, where the entrance $V_{1/2,1/2}$ potential shows a spherical character and it is practically parallel and resonant with the $H_2^+(v = 2)$–Ar vibronic curve. On the contrary the crossing of $Ar^+(^2P_{1/2}) + D_2$ with $D_2^+(v = 3)$ is located at about 3 Å. In this latter case, the range of the impact parameter values that reacts is much smaller and at the same time the unreactive Π character of the crossing is much more developed.

In our model[55] we assume that the reactivity of the system depends on its ability to reach one of the surfaces describing $X_2^+(v)$ + Ar. The transition probabilities have been calculated using an extended Landau–Zener type theory including quantum mechanical tunneling.[32,55,62] Moreover we can also describe the metastable bound states which may arise when the system makes a transition to the charge-transfer state in the exit

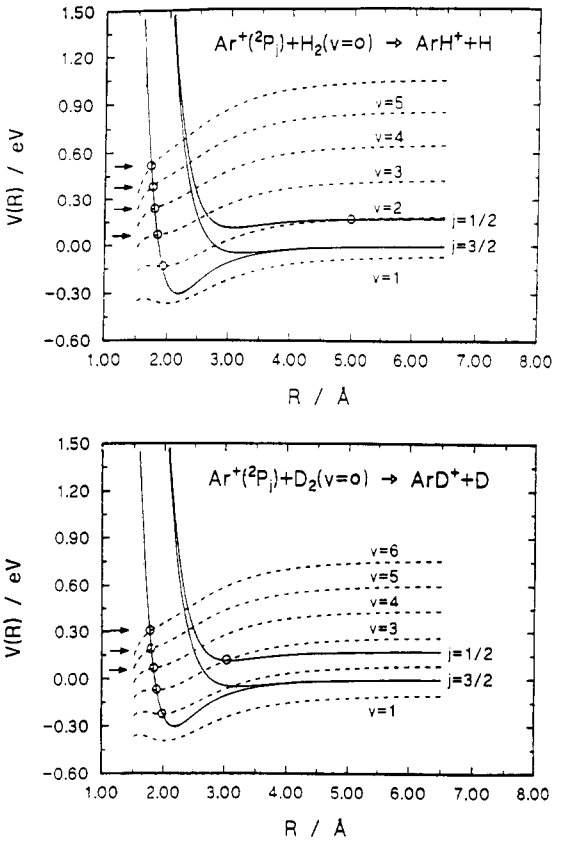

Figure 7. Collinear cuts of entrance channels of the potential energy surfaces for (top) Ar^+ interacting with H_2 and (bottom) Ar^+ interacting with D_2. Solid lines represent the $Ar^+(^2P_j)$–X_2 potential curves: For each isotope system, the lowest curve indicates $V_{3/2,1/2}$, the middle $V_{3/2,3/2}$, and the highest $V_{1/2,1/2}$ (see the text). Dashed lines represent the X_2^+ (v = 1, 2, ...)–Ar vibronic curves, correlating with the products. Circles indicate crossings which are adiabatically avoided by symmetry. Arrows mark endothermic crossings.

channel. If the $X_2^+(v)$ + Ar state has an energy higher than the collision energy then the system is forced to go back to the crossing. This oscillation generates a metastable bound state.

The energy dependence of calculated cross sections is shown in Figures 8 and 9. These values are calculated by integrating the transition probabilities over the impact parameters, therefore taking into account several partial waves. In agreement with the experimental results and their interpretation, the calculated cross sections show a clear structure. The high-frequency oscillations are due to the quasi-bound states discussed previously.

The direct fit of the experimental data is neither in the possibility of the model, nor in the spirit of our calculations. However, the qualitative reproduction of experimental features allows one to obtain relevant information on the potential energy surfaces and on the reaction dynamics. This will be discussed in detail in a future paper.[55]

In conclusion, it has to be mentioned that recent merged-guided ion-beam measurements[24] failed to reproduce the structure reported by us and discussed above. The effective rate coefficients measured by these authors show a monotonic energy dependence, their values are practically constant for collision energy lower than 10 meV, and roughly a factor of 2 larger than low-temperature data[49] at about 1 meV. As a consequence

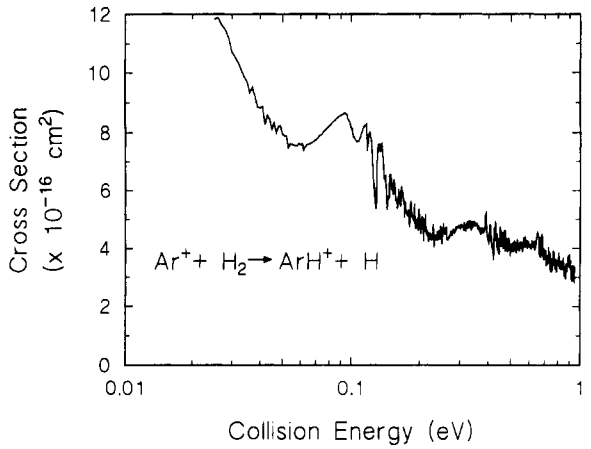

Figure 8. Calculated cross section as a function of the collision energy for the reaction $Ar^+ + H_2 \rightarrow ArH^+ + H$. Numerical values are obtained by integrating the transition probability over the impact parameter.

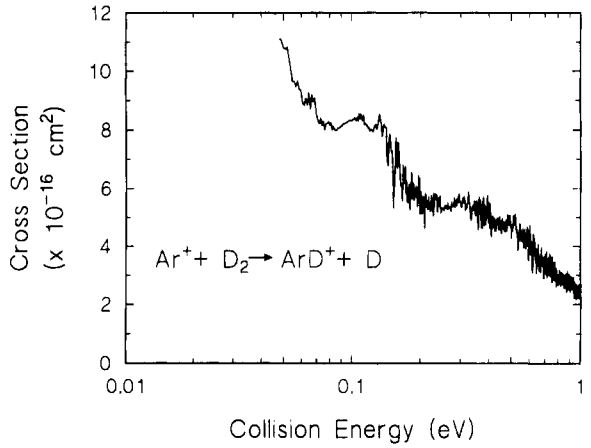

Figure 9. Calculated cross section as a function of the collision energy for the reaction $Ar^+ + D_2 \rightarrow ArD^+ + D$. Numerical values are obtained by integrating the transition probability over the impact parameter.

merged beam data indicate a weaker positive-energy dependence than observed from other laboratories (see Figure 2). In view of the superior performances of the merged-beam configuration, at the present it is difficult to identify causes of these discrepancies. Moreover, for other systems (see N^+–D_2 in the following) merged–guided ion-beam and crossed-beam results agree quite well. As already discussed both of the experimental instruments have respective disadvantages. In the merged geometry the poor definition of the scattering region might result in the smoothing of narrow features due to undesirable background signal. On the other hand, discrimination effects might be critical in the crossed-beam configuration, due to a possible unfavorable center-of-mass motion. As an example, we wonder if the observed structure might be amplified by selective discrimination of state-specific products scattered at specific angles.

B. $N_2^+ + X_2 \rightarrow N_2X^+ + X$, X = H, D

The reactions

$$N_2^+ + H_2 \rightarrow N_2H^+ + H \quad (23)$$

$$N_2^+ + D_2 \rightarrow N_2D^+ + D \quad (24)$$

have been recently reinvestigated.[27,63] Many of the early experimental results come from rate constant measurements at thermal energies.[64] More recently the temperature dependence of the rate constant has been determined from 70 K down to about 15 K,[65,66] whereas the energy dependence of the cross sections has been measured in the whole range from thermal to 10-eV center-of-mass energy.[63] This last study shows that above 0.1 eV the cross section exceeds the prediction of the Langevin model, again indicating that a more complex mechanism is operative in exothermic reactions too. Once more the coupling between the two charge-transfer states plays a fundamental role.

State-selected experiments[67-69] indicate that the reactants $X_2^+ + N_2$ correlate diabatically (without charge transfer) with the $N_2X^+ + X$ products, whereas $N_2^+ + X_2$ react adiabatically, via the charge-transfer intermediate $N_2 + X_2^+$. In other words the reactions of N_2^+ with hydrogen and deuterium can be thought to proceed according to the following scheme:

$$N_2^+ + X_2 \rightarrow N_2 + X_2^+ \rightarrow N_2X^+ + X \quad (25)$$

In fact while the reactions of N_2^+ do not depend on the ion's vibrational state, a strong dependence is observed for the reactions of X_2^+. The fact that the internal energy of the two charge-transfer complexes influences in different ways the reactivity allows one to understand how the two states are coupled to the products and, finally, indicates that the $X_2^+ + N_2$ surface is the one which correlates with the products directly.

These arguments indicate a strong analogy between the present system and the $(Ar–X_2)^+$ previously discussed. From the point of view of the electronic states, the N_2^+–X_2 system is simpler since only one potential energy surface is associated with the reactants as compared to the three surfaces which have to be considered in the case of Ar^+–X_2. However, due to the nitrogen's molecular nature, a much larger number of reactants' relative orientations have to be considered. A further complication is that the vibronic states should, in principle, include the vibrational levels of both the molecules. However, in order to develop a simple reaction model, we neglect the vibrational excitation of N_2 in the intermediate complex. In other words, we assume that the charge-transfer reaction (first step in expression 25), proceeds as follow:

$$N_2^+(v = 0) + X_2(v = 0) \rightarrow N_2(v = 0) + X_2^+(v) \quad (26)$$

that is only the vibrational states of X_2^+ can be populated.

This assumption can be justified by considering the role of the Franck–Condon factors in the charge-exchange process. Transitions between the vibrational levels of $X_2(X)$ and those of $X_2^+(X)$ are favored by 1 order of magnitude with respect to the corresponding N_2–N_2^+ transitions. Hereafter we will always assume that N_2 and N_2^+ are in their ground vibrational state.

Experimental results for the integral cross sections of reactions 23 and 24 are shown in Figures 10 and 11 as a function of the relative energy. In the same figures, the trial function σ (eq 18), used to fit the experimental data, after proper convolution with the experimental energy distribution, is shown by the dashed line. The corresponding fit is shown by the solid line. Following the arguments presented in section III, we have

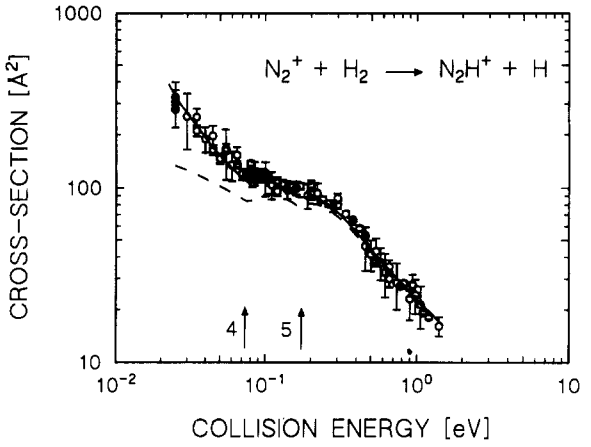

Figure 10. Circles with error bars are experimental, effective cross sections (see eq 3). The dashed line is a parametrized function (see eq 18) used to fit experimental data after proper convolution over experimental conditions. Results of this operation are indicated by the solid line. Vertical arrows indicate bandheads corresponding to the lowest energy crossings between the $N_2^+ + H_2$ curve and the $H_2^+(v) + N_2$ curves labeled by the number v (see text for more details). The absolute scale is obtained by normalization with published data.

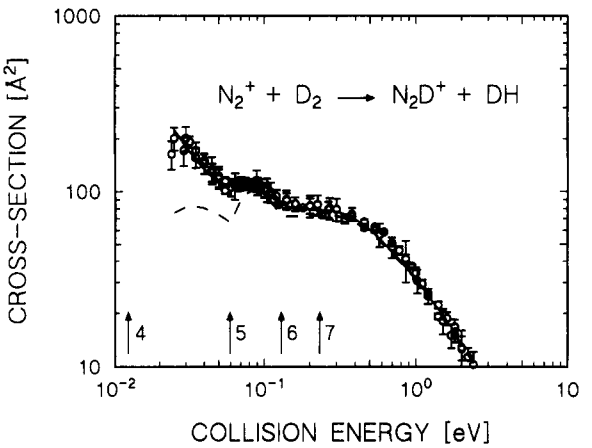

Figure 11. Circles with error bars are experimental, effective cross sections (see eq 3). The dashed line is a parametrized function (see eq 18) used to fit experimental data after proper convolution over experimental conditions. Results of this operation are indicated by the solid line. Vertical arrows indicate bandheads corresponding to the lowest energy crossings between the $N_2^+ + D_2$ curve and the $D_2^+(v) + N_2$ curves labeled by the number v (see text for more details). The absolute scale is obtained by normalization with published data.

compared our data with previously published results. However it should be noted that for energies below about 25 meV, the result of our fit is not very sensitive to the specific form of σ. Therefore σ has been chosen in such a way to reproduce the low-temperature rate constants reported by Rowe et al.[65] and by Randeniya and Smith,[66] as well as our own data.

In Figure 12 we compare literature data[63,70,71] with the results obtained by convoluting σ with the energy distribution function of a beam–cell experiment.[36,37] Although a satisfactory agreement exists between the different sets of data, it is evident that low-energy features are completely lost in beam–cell experiments. Rate constants calculated by means of eq 19 and experimental values from other laboratories[64-66,72] are shown in Figure 13. A good agreement exists over the

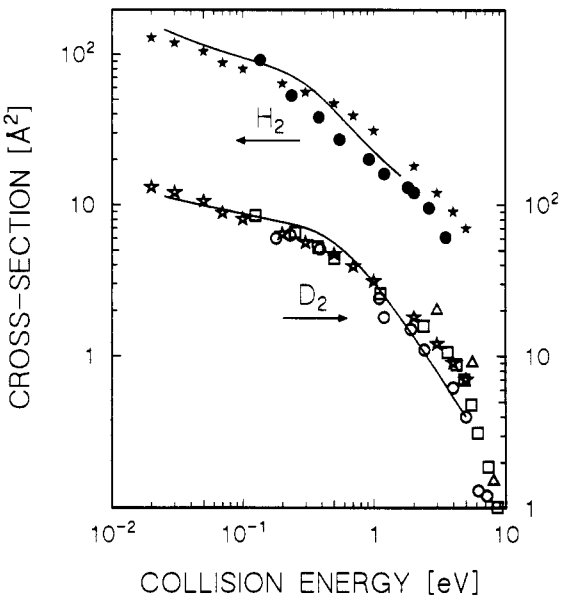

Figure 12. Solid lines are values obtained by convoluting the parametrized function used to fit experimental data (dashed lines in Figures 10 and 11) with the energy distribution function of a beam–cell experiment. The different symbols are literature data: stars, ref 63; squares, ref 70; circles, ref 71. Solid symbols refer to H_2, open symbols to D_2.

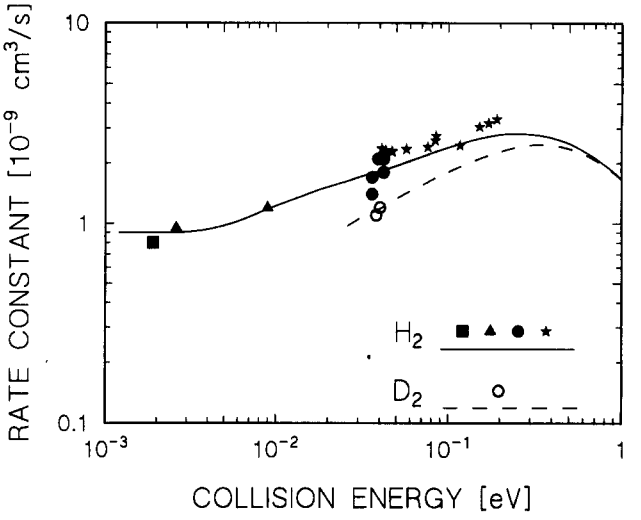

Figure 13. Comparison between rate constants calculated by means of eq 19 (solid line H_2, dashed line D_2) and literature data: stars, ref 72; circles, ref 64; triangles, ref 65; squares, ref 66.

whole energy range with the exception of the very-low-energy data (not shown in Figure 13). In fact at the lowest temperatures a completely different reaction mechanism is operative[66] that has not been taken into account when the functional form of σ had been determined.

The cross sections in Figures 10 and 11 show a structured energy dependence that is different for the two isotopic systems. Aside from the difference in the features' location, the deuterated system shows a broader shoulder. This fact supports the idea that the reaction proceeds via transitions from the $N_2^+ + X_2$ to the $X_2^+ + N_2$ diabatic surfaces. In fact if any major role is played by the vibrational states of X_2^+ then the cross sections for reactions 23 and 24 should be different. As in the case of the Ar^+ reactions with hydrogen and deuterium we correlate the features in the cross section

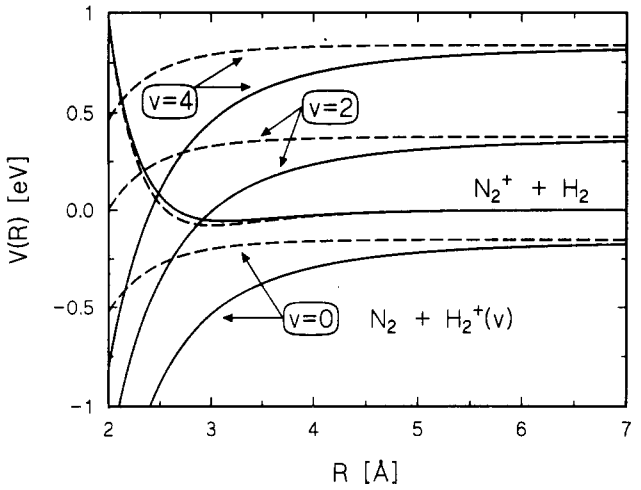

Figure 14. Collinear cuts of entrance channels of the potential energy surfaces for $N_2^+(v = 0) + H_2(v = 0)$ and $H_2^+(v) + N_2(v = 0)$. For sake of clarity only the $v = 0$, 2, and 4 curves are shown. The solid lines refer to the parallel orientation of the neutral molecule with respect to the intermolecular axis ($C_{\infty v}$). The dashed lines refer to the perpendicular configuration (C_{2v}).

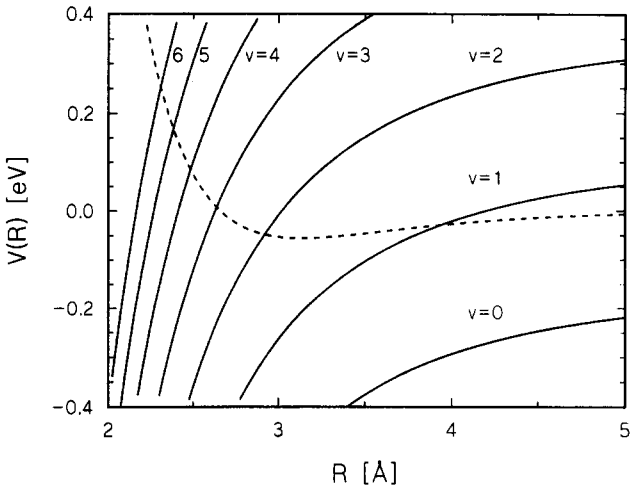

Figure 15. Collinear cuts of entrance channels of the potential energy surfaces for $N_2^+(v = 0) + H_2(v = 0)$ and $H_2^+(v) + N_2(v = 0)$ for the most attractive configuration (H_2 perpendicular, N_2 parallel to the intermolecular axis).

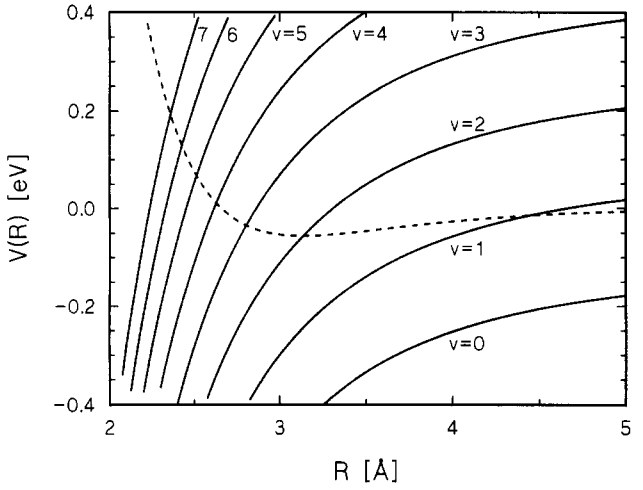

Figure 16. Collinear cuts of entrance channels of the potential energy surfaces for $N_2^+(v = 0) + D_2(v = 0)$ and $D_2^+(v) + N_2(v = 0)$ for the most attractive configuration (D_2 perpendicular, N_2 parallel to the intermolecular axis).

to the opening of endoergic reactive channels via excited vibronic states of the charge-transfer intermediate complex.

Due to the strong quadrupole term of the nitrogen molecule, the interaction potential between X_2^+ and N_2 is quite anisotropic. As previously anticipated several collision geometries have to be considered to take into account the effect of different mutual orientations of the molecular axes. Now the location of the avoided crossings will depend on the particular collision geometry and therefore each vibronic state become accessible, through different geometries, over a wide range of collision energies. From this qualitative discussion it is already possible to understand why the features in the energy dependence of the cross section are in this case broader and less resolved unlike systems characterized by a more isotropic potential.

A more precise understanding of the reaction dynamics can be achieved by estimating quantitatively the interaction potentials. For the entrance potential $N_2^+ + X_2$ we used a Morse functional form whose parameters were determined by the Cappelletti–Liuti–Pirani correlation rules[60] previously used for the $Ar^+ + X_2$ system. In particular we have obtained the well depth ϵ and its location R_m. These values depend on the relative orientation of the two molecules due to the different molecular polarizabilities, parallel or perpendicular to the molecular axis. When X_2 is parallel to the intermolecular axis (symmetry $C_{\infty v}$), we estimated $\epsilon = 56$ meV and $R_m = 3.13$ Å. For the perpendicular geometry (symmetry C_{2v}), we got $\epsilon = 78$ meV and $R_m = 3.01$ Å.

For the intermediate complex $X_2^+ + N_2$ only the charge-induced dipole and the charge-quadrupole terms have been considered:

$$V(r,\theta) = -q^2\alpha/2r^4 + (3\cos^2\theta - 1)[-q^2(\alpha_\parallel - \alpha_\perp)/6r^4 + Qq/2r^3] \quad (27)$$

where r is the intermolecular distance, θ the angle between r and the N_2 axis, q the ion charge, α the N_2 spherically averaged polarizability, and Q the nitrogen quadrupole moment.

This assumption is justified by the following reasons: (i) the reaction $X_2^+ + N_2 \rightarrow N_2X^+ + X$ is exoergic, and (ii) in the energy range explored in this experiment, products $N_2X^+ + X$ are favored by more than 1 order of magnitude over the concurrent charge-transfer channel leading to $X_2^+ + N_2$.[67,68] This means that once the crossing is reached, most likely the system proceeds in the chemical rearrangement channel rather than in the charge-transfer one. To take into account this latter process, one should introduce repulsion in the proposed scheme.

Figure 14 shows the diabatic vibronic curves obtained as collinear cuts of the proposed potential energy surfaces for two nitrogen orientations. Here it is assumed that the molecular orientations do not change during the charge-transfer process. Solid lines correspond to the parallel orientation of the molecule with respect to the intermolecular axis, while dashed lines correspond to the perpendicular orientation. Figures 15 and 16 show the entrance channels for reactants in the most attractive configuration.

The analysis of these curves immediately provides a few interesting conclusions. The first is that the

vibronic surface corresponding to $X_2^+(v = 0)$ never crosses the reactants' surface and therefore, in this model, it does not contribute to the reactivity.

This fact is consistent with the finding that at thermal energies more than 80% of the N_2H^+ ions are produced vibrationally excited and more than 50% are in the vibrational state $v \geq 2$.[73] The decoupling between $X_2^+(v = 0) + N_2$ and $N_2^+ + H_2$ is also consistent with the experimental observation that the cross section for the charge-transfer reaction $X_2^+(v) + N_2 \rightarrow N_2^+ + H_2$ increases by about a factor of 6 for hydrogen and 9 for deuterium when X_2^+ is excited from $v = 0$ to $v = 1$.[67]

The second important finding is the existence of a few exoergic crossings, corresponding to the vibronic curves $v = 1$ and $v = 2$ for H_2 and $v = 1$–3 for D_2. This explains the reactivity at very low energies.

Schultz and Armentrout[63] found that at thermal energies the reaction proceeds at the classical Langevin rate. However increasing the collision energy above 0.1 eV the cross section is higher than the values predicted by the classical ion–molecule capture theory. This finding is noteworthy, since for nonpolar molecules, only downward deviations have been reported.

These authors discussed two possible explanations for such intriguing behavior. The first is based on the idea that the actual potential energy surface is more attractive than the ion-induced dipole potential, due to additional terms as the ion-quadrupole potential.

The second explanation takes into account the needing to switch the charge state, in order to correlate with the products. As already discussed, following an electron jump, the reaction occurs on the $X_2^+ + N_2$ potential energy surface. Due to the larger polarizability of N_2 with respect to X_2, the collision cross section for the $X_2^+ + N_2$ interaction is larger than that calculated on the $N_2^+ + X_2$ potential surface.

We suggest that at hyperthermal energies the reaction can proceed through the endothermic avoided crossings. The greater than Langevin reactivity observed in the beam–cell experiment,[63] might be therefore just a low-resolution image of the lumps due to the successive overcoming of energy barriers through the endothermic avoided crossings.

Note that in the $(N_2–X_2)^+$ system all the crossings are avoided (there are no symmetry constraints) due to the $^2\Sigma_g^+$ character of the N_2^+ ground state.

As already discussed the location of the crossings changes with the collision geometry and, as suggested by Schultz and Armentrout,[63] with the reactants' rotational energy too. As a consequence instead of a single threshold an energy band has to be considered, corresponding to which different reactants' configurations become reactive. For each band an effective threshold is given by its lower limit, hereafter called bandhead. This corresponds to the most attractive configuration, that is to the collinear geometry of N_2 with respect to X_2^+, see Figures 15 and 16. Bandheads are indicated by vertical arrows in Figures 10 and 11. In the hydrogen reaction, the first dip at about 70 meV corresponds to the crossing with the vibronic curve which correlates to a large distance, with $H_2^+(v = 4) + N_2$. Remarkably, the state-selected experiment by Lee's group[67] shows that for the reaction $H_2^+(v) + N_2 \rightarrow N_2H^+ + H$ at 0.5-eV collision energy, the most efficient vibrational state between 2, 3, and 4 is just the latter. For D_2 the first dip is related to $v = 5$. In agreement with the present interpretation, the spacing between the two successive dips in the hydrogen reaction ($v = 4$ and $v = 5$) is larger than the one in the deuterium reaction ($v = 5$ and $v = 6$). Bandheads corresponding to higher crossings are closer to each other. Therefore individual contributions are not resolved in our experiment. In particular this seems to be the case for the deuterated system due to the minor vibrational spacing. As a result, above about 200 meV only one broad structure is resolved.

In conclusion the experimental data support the idea that the reaction proceeds via transitions from the $N_2^+ + X_2$ to the $X_2^+ + N_2$ diabatic surfaces. The broad features observed in the energy dependence of the cross section are attributed to the opening of new reactive channels via excited vibronic curves of the intermediate charge-transfer complex. Reaction dynamics is complicated by the fact that several collision geometries have to be considered due to the strong anisotropy of the $X_2^+ + N_2$ interaction potential.[63] A direct consequence of such anisotropy is that the thresholds for the opening of each vibronic state of the intermediate complex depend on the collision geometry. The estimate of the interaction potentials and the proposed model for the reaction dynamics yield a consistent explanation of the fact that product ions are internally excited.

C. $Ar^+ + N_2 \rightarrow N_2^+ + Ar$

The electron-transfer reaction is probably the simplest nonadiabatic process, since there is no atom rearrangements.

In particular the charge transfer of Ar^+ to N_2 has attracted for many years experimentalists[74–78] and theoreticians.[79–81]

One of the reasons for such interest is the state-selective production of N_2^+. In fact, although the formation of $N_2^+(X, v = 0)$ is exothermic by 0.179 eV, the most likely product ion, at low energy, is $N_2^+(X, v = 1)$, whose production requires 0.092 eV for the reaction of $Ar^+(^2P_{3/2})$.

The nascent product rotational state distribution shows interesting features too. In particular the rotational populations of the ground and the first vibrational states of N_2^+ cannot be described by a single Boltzmann temperature, but have low- and high-energy components.[81,82] Other remarkable aspects of this reaction include the different reactivity of the two spin–orbit states of Ar^+,[76,83–85] the influence of the rotational energy on the reactivity,[78] and some evidence for dynamic resonances.[6] However, in spite of the considerable effort, significant discrepancies exist among the results of different laboratories. The large scatter in the experimental data calls for further data collection.

In addition to establish a new set of integral cross sections from 0.09 eV up to 60 eV, our aim was also to measure the energy threshold at about 0.09 eV for the formation of $N_2^+(X, v = 1)$. Beside the intrinsic interest, the observation of this well-know channel constitutes a significant test for any high-resolution apparatus.

Charge-transfer cross sections are shown in Figure 17 as a solid line, together with a few data from other laboratories.[46,76,79,86–90] As already discussed in section III, a direct comparison among such values is, in

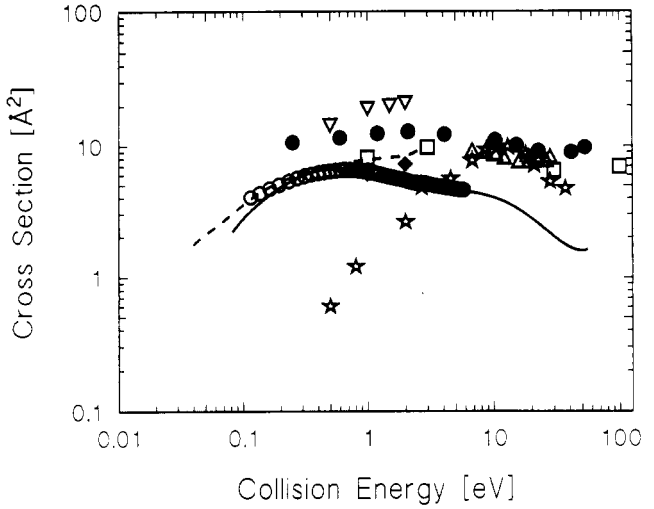

Figure 17. Cross sections (see eq 4) for the charge-transfer reaction $Ar^+ + N_2$ as a function of relative energy. Results of this work are indicated by the continuous line. The experimental relative values have been scaled on the absolute values of Dalleska and Armentrout (ref 90), open circles. Other results from literature are shown as follow: dashed line, ref 46 (rate constant values k converted to cross sections by using the relation $\sigma = k/g$); solid circles, ref 76; open squares, ref 79; solid diamonds, ref 86; stars, ref 87; inverted open triangles; ref 88; open triangles, ref 89.

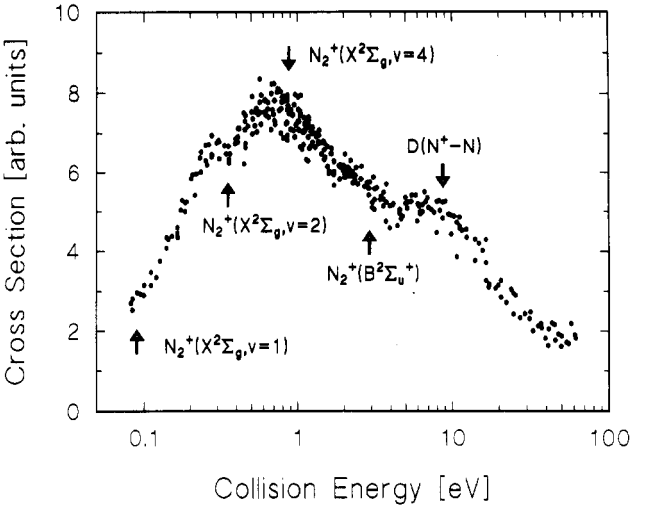

Figure 18. Cross sections (see eq 4) for the charge-transfer reaction $Ar^+ + N_2$ as a function of relative energy. Arrows indicate the thermodynamic onset for the formation of the N_2^+ product ions in different states and the N_2^+ dissociation energy.

principle, misleading since the resolving power of each experiment should be taken into account. However effects due to the energy resolution are actually very important only at energies below 1 eV. Therefore, for the present system the comparison among the different data sets is significant in most of the energy ranges investigated.

We have normalized our relative values on the absolute cross sections obtained in a recent experiment by Dalleska and Armentrout[90] (open circles in Figure 17). They cooled the scattering cell to about 100 K, thus reducing the Doppler broadening. Due to the unfavorable projectile–target mass ratio, for this system the energy resolution of our crossed-beam apparatus is only slightly better than that achievable by using a low-temperature scattering cell. As a consequence, in first approximation the results of the two respective experiments can be directly compared without any further convolution procedure. In this case we have to use eq 4 to estimate the cross sections. Therefore the data shown in Figure 17 are an average over the reactants' energy distribution that, for the present experiment, has a fwhm of about 0.08 eV. A good agreement is evident between the results of the two different high-resolution experimental apparatus (crossed-beam and beam–low-temperature scattering cell). The correspondence is quite encouraging despite of discrepancies with other data.

Among the most recent and reliable experimental data are those of Liao et al.[76] These values are roughly a factor of 2 larger and have a somehow different energy dependence. A common problem in guided ion-beam apparatus is that product ion collection may be incomplete for charge-transfer reactions.[92] Therefore absolute values may differ by as much as a factor of 2. However the absolute values measured by Dalleska and Armentrout agree quite well at low energies with data of Dotan and Lindinger[46] (dashed line in Figure 17). These authors measured rate constants k, which have been converted to cross sections by using the relation $\sigma = k/g$.

Primary merits of the elegant experiment of Liao et al.[76] consist of probing the different reactivity of the two spin–orbit states and of providing state analysis of the products. Considering differences in the experimental apparatus, the different energy resolution, and a possible difference in the internal state composition of the primary ions, we feel the overall agreement with the data of Liao et al. is satisfactory.

Experimental cross sections show a typical endothermic shape. The apparent threshold at about 0.09 eV is clearly related to the asymptotic energy value of $N_2^+(X, v = 1)$. Note that some smoothing effects result from the energy spread of the two beams and the presence of $Ar^+(^2P_{1/2})$. The present data confirm that at low energies the reaction mainly produces the nitrogen ion in the first vibrational state.[74–76,82,91] This remarkable state selectivity has been discussed and rationalized on the basis of a curve-crossing mechanism.[79–81,93]

Some other features of the cross section are observed and deserve a few comments. In Figure 18 an enlarged plot of the cross section versus the collision energy is shown. A clear change in the slope between 0.3 and 0.4 eV corresponds to the threshold for the production of $N_2^+(X, v = 2)$. Interestingly, both Liao et al.[76] and Birkinshaw et al.[91] found that $N_2^+(X, v = 2)$ is produced at these energies by the charge-transfer reaction with Ar^+.

The maximum cross section is reached around 0.8 eV. As a consequence the production of $N_2^+(X)$ in vibrational states higher than $v = 4$ is less efficient than in lower states. This conclusion is fully supported by the experiments of Futrell and co-workers.[6,91] These authors have found that in the energy window between about 0.8 and 1.3 eV, all the energetically accessible vibrational states of $N_2^+(X)$ are formed. On the contrary at higher energies the reaction generates dominantly the $v = 1$ vibrational state, despite the fact that the energy is sufficient to populate several vibrational states.

A second hump at about 4 eV suggests the opening of a new product channel. The state which has the closer thermodynamic threshold is $N_2^+(B^2\Sigma)$ and we speculate about the possible formation of this electronically excited state. Some evidence for the production of electronically excited states by the title reaction has been discussed recently.[94]

Above 9 eV the falloff of the N_2^+ product is most probably correlated with the onset of the dissociative charge transfer, producing $N^+ + N$. The change in the slope of the cross section corresponds in fact to the thermodynamic threshold (8.7 eV) for dissociation of N_2^+. By direct experimental observation, Flesch and Ng[94] have shown that the appearance energy for the production of N^+ by collisions of Ar^+ ions with nitrogen is in agreement with the thermochemical threshold for the reaction $Ar^+ + N_2 \rightarrow N^+ + N + Ar$. They also concluded that N^+ ions are predominantly produced by the predissociation of electronically excited states of N_2^+. This conclusion supports our belief that electronically excited states of N_2^+ can be populated by the charge-transfer reaction of Ar^+ to N_2.

D. $N^+ + D_2 \rightarrow ND^+ + D$

The reactions of N^+ with hydrogen and deuterium are very important in astrochemistry, especially due to their possible role in the synthesis of ammonia in the interstellar space. In fact a proposed route to the formation of NH_3 is the reaction sequence:[95,96]

$$(a)\ N^+ + H_2 \rightarrow NH^+$$

$$(b)\ NH^+ + H_2 \rightarrow NH_2^+$$

$$(c)\ NH_2^+ + H_2 \rightarrow NH_3^+$$

$$(d)\ NH_3^+ + H_2 \rightarrow NH_4^+$$

$$(e)\ NH_4^+ + e \rightarrow NH_3$$

Other reasons of interest include the possible dependence of the reactivity on the rotational and spin–orbit energies. Considerable effort has been dedicated to the calculation of potential energy surfaces and related trajectories studies.[97]

A key problem is the reaction's energetics. In 1985 Adams and Smith[98] measured a positive energy dependence of the rate coefficients and established that the reactions of N^+ with both hydrogen and deuterium are endothermic of a few tens of millielectronvolts. They also discarded the possibility that the experimental endothermicity is an activation energy, by showing that differences in thermicities for the different isotope reactions can be accounted for by differences in the vibrational zero-point energies of the reactant and product molecules. One important reason for establishing precise values for reaction endothermicities is that, by these numbers, the heat of formation and the bond energy of NH^+ may be estimated better than by spectroscopic[99] or ab initio[100] methods.

In spite of considerable effort,[101-104] reaction endothermicities are still not precisely known, since estimated values in the case of H_2 range from 11 to 33 meV, whereas for D_2 the values range from 33 up to 61 meV.

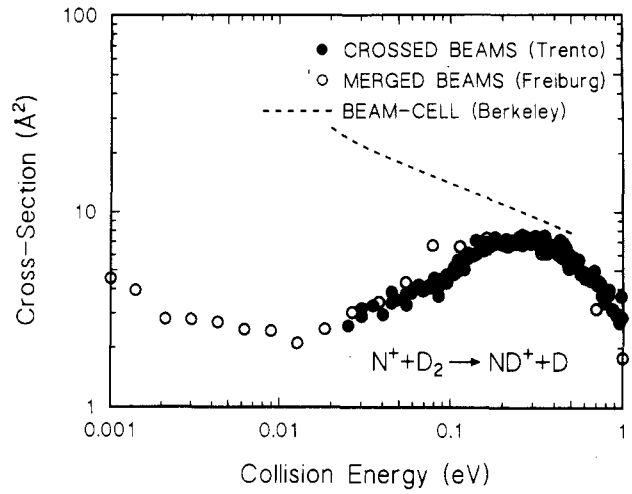

Figure 19. Cross sections (see eq 4) for the reaction $N^+ + D_2 \rightarrow ND^+ + D$: solid circles, this work; open circles, ref 105; dashed line, ref 104.

The energy dependence of the cross section has been measured in a beam–cell apparatus.[104] Unfortunately the energy threshold has not been observed, due to the insufficient energy resolution, but estimated by the convolution of a model cross section over the energy distribution of the reactants. Modeling the energy threshold behavior introduces a large uncertainty. Low-temperature measurements of the thermal rate constant[101-103] indicate that the threshold for the hydrogen reaction is close to 17 meV. This number agrees also with a theoretical calculation based on a dynamically biased statistical theory.[103] This value is too low to be measured in our crossed-beam apparatus. On the contrary, due to its higher value, the measurement of the threshold for the deuterium reaction is an ideal goal for an high-resolution apparatus. Another advantage of deuterium with respect to hydrogen is that the rotational cooling is more effective. At the liquid nitrogen temperature of the supersonic beam, 66.7% of the D_2 molecules are in the rotational state $J = 0$ and 33.3% in the $J = 1$ state.

Using rotationally cooled molecules is important in this system since the endothermicity is close to the rotational quanta and the rotational energy is known to drive the reaction.[102,103]

Experimental data are shown in Figure 19. Also in this case we used eq 4 to estimate the cross section, to avoid, in a first stage, the convolution procedure over the reactants' energy spread. The reason for that, besides simplicity, is the need to compare, on the same plot, our data and those obtained in a recent experiment by Gerlich in his merged-beam apparatus.[105] This comparision is particularly significant since although both our and Gerlich's apparatus are suitable for high-resolution measurements, they adopt different geometries (see discussion in sections III and V.A). Regardless of this fact, a good agreement is evident between our respective results.

The comparision with data from the beam-cell apparatus[104] is of course more problematic, due to the completely different energy resolutions involved. The high-resolution cross section shows a clear endothermic shape. In contrast, no threshold is evident in the low-

resolution beam–cell data set. In this latter case, at low energies, the measured cross section is proportional to $E_{CM0}^{-1/2}$, that is it shows an exothermic behavior!

An important difference between the crossed-beam and the merged-beam experiments lies on the N^+ ions preparation. In our experiment we produce the primary ions in an electron bombardment source and therefore we assume we get a statistical mixture of N^+ spin–orbit states. In Gerlich's experiment, N^+ ions have been stored for 13 ms in 20 K cold helium buffer gas before the production of the ion beam. The agreement between the two data sets implies either that the ions relax very slowly or that the spin–orbit energy of N^+ does not contribute to the reaction. This point is currently under investigation.[106]

If one accounts for the D_2 rotational energy, a tentative threshold of about 35 meV can be derived. Considering that NH^+ production requires about 17 meV, we obtain an experimental difference between the thresholds of the two isotope reactions of about 18 meV, clearly less than the asymptotic difference in zero-point energies. This conclusion is supported by phase-space theory calculations.[105] The 17-meV value for the threshold, assumed as a free parameter, yields a good agreement between calculated[105] and experimental rate constants[102,105] for $N^+ + H_2$. If the endothermicity for the deuterated analog is then calculated by adding the asymptotic difference in zero-point energies, a value of about 45 meV is found. By using this number, calculated rate constants for the $N^+ + D_2$ reaction are smaller than the experimental ones. This indicates that the threshold of 45 meV is probably overestimated. If the difference between the threshold values does not coincide with the difference in zero-point energies, then the observed energy dependence is not due to a genuine endothermicity but probably to an energy barrier on the potential energy surface.

VI. Conclusions

In this paper we have shown by a few examples that an experimental setup in which a supersonic molecular beam is crossed at 90° with the radio frequency guided ion beam offers the possibility to measure cross sections of ion–molecule reactions with high-energy resolution at low collision velocities. The energy dependence of the cross section, if known with sufficient resolution, may furnish great insight into the reaction dynamics. In particular for nonadiabatic reactions, the manner in which different states are coupled to each other as a function of the collision energy may be directly probed. For the reactions discussed in this paper the high-resolution measurements indicate a monotonic energy dependence of the cross section. The explanation of this finding requires a novel theoretical approach which fully takes into account fine structure and vibrational effects.

Several improvements of the present apparatus are possible and planned to be made in the near future. They should increase the sensitivity, the energy resolution, and the overall reliability of the machine. A few drawbacks of this technique should be mentioned too. Major limitations of the crossed-beam's configuration are related to the very small dimensions of the interaction region and to possible detection problems for product ions which are back-scattered in the laboratory reference frame. A small interaction region results in a small products signal. Therefore (i) only reactions with cross sections larger than a few angstroms squared can be investigated (ii) an intense primary ions beam is required. As an example, this last fact prevents in most of the cases the possibility to use state-selected primary ions. The second problem, which has already been discussed in the section entitled "Experimental", further limits the range of chemical systems which can be investigated. A particularly careful kinematics analysis should be performed, for example, in charge-transfer reactions, since the product ions tend to move in the same direction as their neutral precursor, that is perpendicular to the detector. All these problems made the experiment here presented a not routine technique.

A detailed understanding of the reaction dynamics in ion–molecule reactions can be obtained only by combining information from different and often complementary experimental techniques. These include collisional, spectroscopic, and coincidence methods.[107] We hope that our recent work in the narrow topic of high-resolution integral cross-section measurements may contribute, together with results from other laboratories, to some understanding of the elementary processes in ion–molecule reactions.

VII. Acknowledgments

The author gratefully acknowledges helpful discussions with P. B. Armentrout and D. Gerlich. I am very much in debt to my former students Franco Boldo, Fausto Eccher, Mauro Filippi, and Stefano Longano, who have in different periods helped to build the apparatus, and Yvonne Soldo, who contributed to the theoretical interpretation. I have greatly benefited from a collaboration with the Molecular Dynamics Group of the Chemistry Department at the Universitá di Perugia and in particular with David Cappelletti, Fernando Pirani, and Vincenzo Aquilanti to whom I am grateful for their teaching. Finally special thanks are due to my colleagues in Trento, Davide Bassi, Oleg Dmitrijev, and Mario Scotoni, for their priceless work and help, and to Roberta Guardini, for this manuscript's preparation.

References

(1) *Techniques for the study of ion-molecule reactions*; Farrar, J. M., Saunders, W. H., Jr., Eds.; Wiley: New York, 1988.
(2) Burley, J. D.; Ervin, K. M.; Armentrout, P. B. *J. Chem. Phys.* **1987**, *86*, 1944.
(3) Light, J.; Ross, J.; Shuler, K. *Kinetic Processes in Gases and Plasmas*; Hochstim, A., Ed.; Academic Press: New York, 1969; p 281.
(4) Zhang, J. Z. H.; Yeager, D. L.; Miller, W. H. *Chem. Phys. Lett.* **1990**, *173*, 489.
(5) Pollard, J. E.; Syage, J. A.; Johnson, L. K.; Cohen, R. B. *J. Chem. Phys.* **1991**, *94*, 8615.
(6) Rockwood, A. L.; Howard, S. L.; Wen-Hu, Du; Tosi, P.; Lindinger, W.; Futrell, J. H. *Chem. Phys. Lett.* **1985**, *114*, 486.
(7) Parlant, G.; Gislason, E. A. *J. Chem. Phys.* **1987**, *86*, 6183.
(8) Dressler, R. A.; Gardner, J. A.; Salter, R. H.; Wodarczyc, F. J.; Murad, E. *J. Chem. Phys.* **1990**, *92*, 1117.
(9) Ng, C. Y. *Techniques for the study of ion-molecule reactions*; Farrar, J. M., Saunders, W. H., Jr., Eds.; Wiley: New York, 1988.
(10) Farrar, J. M. *Techniques for the study of ion-molecule reactions*; Farrar, J. M., Saunders, W. H., Jr., Eds.; Wiley: New York, 1988.
(11) Futrell, J. H. *Adv. Chem. Phys.* **1992**, *82*, 501.
(12) Neidner-Schatteburg, G.; Toennies, J. P. *Adv. Chem. Phys.* **1992**, *82*, 553.
(13) Trujillo, S. M.; Neynaber, R. H.; Rothe, E. W. *Rev. Sci. Instrum.* **1966**, *37*, 1655.

(14) Gentry, W. R.; McLure, D. J.; Douglass, C. H. *Rev. Sci. Instrum.* **1975**, *46*, 367.
(15) Douglass, C. H.; Ringer, G.; Gentry, W. R. *J. Chem. Phys.* **1982**, *76*, 2423.
(16) Teloy, E.; Gerlich, D. *Chem. Phys.* **1974**, *4*, 417.
(17) Tosi, P.; Fontana, G.; Longano, S.; Bassi, D. *Int. J. Mass Spectrom. Ion Processes* **1989**, *93*, 95.
(18) For a comprehensive review on inhomogeneous radio frequency fields, see: Gerlich, D. *Adv. Chem. Phys.* **1992**, *82*, 1.
(19) Armentrout, P. B. *Comments At. Mol. Phys.* **1988**, *22*, 133.
(20) Stevenson, D. P.; Schissler, D. O. *J. Chem. Phys.* **1958**, *29*, 282. Gioumousis, G.; Stevenson, D. P. *J. Chem. Phys.* **1958**, *29*, 294.
(21) Lindinger, W. *Int. J. Mass Spectrom. Ion Processes* **1987**, *80*, 115.
(22) Ervin, K. M.; Armentrout, P. B. *J. Chem. Phys.* **1985**, *83*, 166.
(23) Gerlich, D.; Disch, R.; Scherbarth, S. *J. Chem. Phys.* **1987**, *87*, 350.
(24) Gerlich, D.; Jitschin, H. J.; Wick, O. *Proceedings of SASP 92, Pampeago/Tesero, Italy, 1992*; Bassi, D., Scotoni, M., Tosi, P., Eds.; Universitá di Trento: Trento, 1992.
(25) Tosi, P.; Boldo, F.; Eccher, F.; Filippi, M.; Bassi, D. *Chem. Phys. Lett.* **1989**, *164*, 471.
(26) Tosi, P.; Eccher, F.; Bassi, D.; Pirani, F.; Cappelletti, D.; Aquilanti, V. *Phys. Rev. Lett.* **1991**, *67*, 1254.
(27) Tosi, P.; Dmitrijev, O.; Bassi, D. *J. Chem. Phys.* **1992**, in press.
(28) Tully, J. C. *Dynamics of Molecular Collisions*; Miller, W. H., Ed.; Plenum: New York, 1976; Part B, p 217.
(29) Aquilanti, V.; Grossi, G. *J. Chem. Phys.* **1980**, *73*, 1165.
(30) Smith, F. T. *Phys. Rev.* **1969**, *179*, 111.
(31) Baer, M. *Chem. Phys. Lett.* **1975**, *35*, 112.
(32) Landau, L. D.; Lifshitz, E. M. *Quantum Mechanics*; Pergamon Press: Oxford, 1965.
(33) Ervin, K. M.; Armentrout, P. B. *J. Chem. Phys.* **1986**, *85*, 6380.
(34) Kuntz, P. J.; Roach, A. C. *J. Chem. Soc., Faraday Trans. 2* **1972**, *68*, 259.
(35) Ervin, K. M.; Armentrout, P. B. *J. Chem. Phys.* **1989**, *90*, 118.
(36) Chantry, P. J. *J. Chem. Phys.* **1971**, *55*, 2746.
(37) Lifshitz, C.; Wu, R. L. C.; Tiernan, T. O.; Terwillger, D. T. *J. Chem. Phys.* **1978**, *68*, 247.
(38) Schlier, C. G. *Chem. Phys.* **1988**, *126*, 73.
(39) Sunderlin, L. S.; Armentrout, P. B. *Chem. Phys. Lett.* **1990**, *167*, 188.
(40) For details on molecular beam methods, see: *Atomic and Molecular Beam Methods*; Scoles, G., Ed.; Oxford University Press: New York, 1988.
(41) Miller, D. R. *Atomic and Molecular Beam Methods*; Scoles, G., Ed.; Oxford University Press: New York, 1988; p 14.
(42) Liao, C. L.; Xu, R.; Nourbakhsh, S.; Flesch, G. D.; Baer, M.; Ng, C. Y. *J. Chem. Phys.* **1990**, *93*, 4832 and references therein.
(43) Gislason, E. A.; Parlant, G. *J. Chem. Phys.* **1991**, *94*, 6598.
(44) Smith, R. D.; Smith, D. L.; Futrell, J. H. *Int. J. Mass Spectrom. Ion Processes* **1976**, *19*, 395.
(45) Kemper, P. R.; Bowers, M. T. *Int. J. Mass Spectrom. Ion Processes* **1983**, *52*, 1.
(46) Dotan, I.; Lindinger, W. *J. Chem. Phys.* **1982**, *76*, 4972.
(47) Rebrion, C.; Rowe, B. R.; Marquette, J. B. *J. Chem. Phys.* **1989**, *91*, 6142.
(48) Bedford, D. K.; Smith, D. *Int. J. Mass Spectrom. Ion Processes* **1990**, *98*, 179.
(49) Hawley, M.; Smith, M. A. *J. Chem. Phys.* **1992**, *96*, 7440.
(50) Chapman, S. *J. Chem. Phys.* **1985**, *82*, 4033.
(51) Baer, M.; Liao, C. L.; Xu, R.; Flesh, G. D.; Nourbakhsh, S.; Ng, C. Y.; Neuhauser, D. *J. Chem. Phys.* **1990**, *93*, 4845.
(52) Baer, M.; Beswick, J. A. *Chem. Phys. Lett.* **1977**, *51*, 360.
(53) Aristov, N.; Armentrout, P. B. *J. Am. Chem. Soc.* **1986**, *108*, 1806.
(54) Tosi, P.; Dmitrijev, O.; Soldo, Y.; Bassi, D.; Pirani, F.; Cappelletti, D.; Aquilanti, V. *Proceedings of SASP 92, Pampeago/Tesero, Italy, 1992*; Bassi, D., Scotoni, M., Tosi, P., Eds.; Universitá di Trento: Trento, 1992.
(55) Tosi, P.; Dmitrijev, O.; Soldo, Y.; Bassi, D.; Cappelletti, D.; Pirani, F.; Aquilanti, V. To be published.
(56) Tanaka, K.; Durup, J.; Kato, T.; Koyano, I. *J. Chem. Phys.* **1981**, *74*, 5561.
(57) Hamdan, M.; Birkinshaw, K.; Twiddy, N. D. *Int. J. Mass Spectrom. Ion Processes* **1984**, *62*, 297.
(58) Aquilanti, V.; Liuti, G.; Pirani, F.; Vecchiocattivi, F. *J. Chem. Soc., Faraday Trans. 2* **1989**, *85*, 955.
(59) Cambi, R.; Cappelletti, D.; Liuti, G.; Pirani, F. *J. Chem. Phys.* **1991**, *95*, 1852.
(60) Cappelletti, D.; Liuti, G.; Pirani, F. *Chem. Phys. Lett.* **1991**, *183*, 297.
(61) Dunning, T. H., Jr.; Hay, P. J. *J. Chem. Phys.* **1978**, *69*, 134.
(62) Nikitin, E. E. *Chemische Elementarprozesse*; Hartmann, H., Ed.; Springer-Verlag: Berlin, 1968; p 43 (in German).
(63) Schultz, R. H.; Armentrout, P. B. *J. Chem. Phys.* **1992**, *96*, 1036.
(64) (a) Aquilanti, V.; Galli, A.; Giardini-Guidoni, A.; Volpi, G. G. *J. Chem. Phys.* **1965**, *43*, 1969. (b) Fehsenfeld, F. C.; Schmeltekopf, A. L.; Ferguson, E. E. *J. Chem. Phys.* **1967**, *46*, 2802. (c) Bowers, M. T.; Elleman, D. D.; King, J., Jr. *J. Chem. Phys.* **1968**, *50*, 1840. (d) Ryan, K. R. *J. Chem. Phys.* **1974**, *61*, 1559. (e) Kim, J. K.; Theard, L. P.; Huntress, W. T. *J.* Chem. *Phys.* **1975**, *62*, 45. (f) Tichy, M.; Rakshit, A. B.; Lister, D. G.; Twiddy, N. D.; Adams, N. G.; Smith, D. *Int. J. Mass Spectrom. Ion Phys.* **1979**, *29*, 231.
(65) Rowe, B. R.; Marquette, J. B.; Rebrion, C. *J. Chem. Soc., Faraday Trans. 2* **1989**, *85*, 1631.
(66) Randeniya, L. K.; Smith, M. A. *J. Chem. Phys.* **1991**, *94*, 351.
(67) Anderson, S. L.; Turner, T.; Mahan, B. H.; Lee, Y. T. *J. Chem. Phys.* **1982**, *77*, 1842.
(68) Koyano, I.; Tanaka, K.; Kato, T.; Suzuki, S. *Faraday Discuss. Chem. Soc.* **1987**, *84*, paper 14.
(69) Henri, G.; Lavollée, M.; Dutuit, O.; Ozenne, J. B.; Guyon, P. M.; Gislason, E. A. *J. Chem. Phys.* **1988**, *88*, 6381.
(70) Turner, B. R.; Fineman, M. A.; Stebbings, R. F. *J. Chem. Phys.* **1965**, *42*, 4088.
(71) Hierl, P. M.; Strattan, L. W.; Wyatt, J. R. *Int. J. Mass Spectrom. Ion Phys.* **1973**, *10*, 385.
(72) Freysinger, W. Private communication.
(73) Villinger, H.; Futrell, J. H.; Saxer, A.; Richter, R.; Lindinger, W. *J. Chem. Phys.* **1984**, *80*, 2543.
(74) Smith, D.; Adams, N. G. *Phys. Rev.* **1981**, *A23*, 2327.
(75) Lindinger, W.; Howorka, F.; Lukac, P.; Kuhn, S.; Villinger, H.; Alge, E.; Ramler, H. *Phys. Rev.* **1981**, *A23*, 2819.
(76) Liao, C. L.; Shao, J. D.; Xu, R.; Flesch, G. D.; Li, Y. G.; Ng, C. Y. *J. Chem. Phys.* **1986**, *85*, 3874.
(77) Futrell, J. H. *Int. J. Quantum Chem.* **1987**, *31*, 133.
(78) Viggiano, A. A.; Van Doren, J. M.; Morris, R. A.; Paulson, J. F. *J. Chem. Phys.* **1990**, *93*, 4761.
(79) Parlant, G.; Gislason, E. A. *J. Chem. Phys.* **1987**, *86*, 6183.
(80) Nikitin, E. E.; Ovchinnikova, M. Ya.; Shalashilin, D. V. *Chem. Phys.* **1987**, *111*, 313.
(81) Clary, D. C.; Sonnenfroh, D. M. *J. Chem. Phys.* **1989**, *90*, 1686.
(82) Sonnenfroh, D. M.; Leone, S. R. *J. Chem. Phys.* **1989**, *90*, 1677.
(83) Kato, T.; Tanaka, K.; Koyano, I. *J. Chem. Phys.* **1982**, *77*, 337.
(84) Hamdan, M.; Birkinshaw, K.; Twiddy, N. D. *Int. J. Mass Spectrom. Ion Processes* **1984**, *57*, 225.
(85) Guyon, P. M.; Govers, T. R.; Baer, T. *Z. Phys.* **1986**, *D4*, 89.
(86) Ong, P. P.; Hasted, J. B. *J. Phys. B* **1969**, *2*, 91.
(87) Mahadevan, P.; Magnuson, G. D. *Phys. Rev.* **1968**, *171*, 103.
(88) Kaneko, Y.; Kobayashi, N.; Konomata, I. *J. Phys. Soc. Jpn.* **1969**, *27*, 992.
(89) Rosenberg, A.; Bregmon-Reisler, H.; Amiel, S. *Int. J. Mass Spectrom. Ion Phys.* **1973**, *11*, 433.
(90) Dalleska, N.; Armentrout, P. B. Private communication.
(91) Birkinshaw, K.; Shukla, A.; Howard, S.; Futrell, J. H. *Chem. Phys.* **1987**, *113*, 149.
(92) Fisher, E. R.; Weber, M. E.; Armentrout, P. B. *J. Chem. Phys.* **1990**, *92*, 2296.
(93) Govers, T. R.; Guyon, P. M.; Baer, T.; Cole, K.; Frölich, H.; Lavollee, M. *Chem. Phys.* **1984**, *87*, 373.
(94) Flesch, G. D.; Ng, C. Y. *J. Chem. Phys.* **1990**, *92*, 2876.
(95) Galloway, E. T.; Herbst, E. *Astron. Astrophys.* **1989**, *211*, 413.
(96) Nejad, L. A. M.; Williams, D. A.; Charnley, S. B. *Mon. Not. R. Astrom. Soc.* **1990**, *246*, 183.
(97) Wilhelmsson, U.; Nyman, G. *J. Chem. Phys.* **1992**, *96*, 5198 and references therein.
(98) Adams, N. G.; Smith, D. *Chem. Phys. Lett.* **1985**, *117*, 67.
(99) Gibson, S. T.; Greene, J. P.; Berkowitz, J. *J. Chem. Phys.* **1985**, *83*, 4319.
(100) Pople, J. A.; Curtiss, L. A. *J. Phys. Chem.* **1987**, *91*, 155.
(101) Luine, J. A.; Dunn, G. H. *Astrophys. J.* **1985**, *299*, L67.
(102) Marquette, J. B.; Rebrion, C.; Rowe, B. R. *J. Chem. Phys.* **1988**, *89*, 2041.
(103) Gerlich, D. *J. Chem. Phys.* **1989**, *90*, 3574.
(104) Ervin, K. M.; Armentrout, P. B. *J. Chem. Phys.* **1987**, *86*, 2659.
(105) Gerlich, D. Private communication.
(106) Tosi, P.; Dmitrijev, O.; Bassi, D.; Wick, O.; Gerlich, D. To be published.
(107) For a review on recent advances in the field, see: *Adv. Chem. Phys.* **1992**, *82* (Ng, C. Y., Baer, M., Eds.).